



Published in final edited form as:

Mech Dev. 2013 ; 130(0): 577–601. doi:10.1016/j.mod.2013.08.001.

The *Drosophila* T-box transcription factor Midline functions within the Notch–Delta signaling pathway to specify sensory organ precursor cell fates and regulates cell survival within the eye imaginal disc

Sudeshna Das^a, Q. Brent Chen^a, Joseph D. Saucier^a, Brandon Drescher^a, Yan Zong^b, Sarah Morgan^b, John Forstall^a, Andrew Meriwether^a, Randy Toranzo^a, and Sandra M. Leal^{a,*}

^a The Department of Biological Sciences, University of Southern Mississippi, United States

^b The Department of Polymer and High Performance Materials, University of Southern Mississippi, United States

Abstract

We report that the T-box transcription factor Midline (Mid), an evolutionary conserved homolog of the vertebrate Tbx20 protein, functions within the Notch–Delta signaling pathway essential for specifying the fates of sensory organ precursor cells. This complements an established history of research showing that Mid regulates the cell-fate specification of diverse cell types within the developing heart, epidermis and central nervous system. Tbx20 has been detected in diverse neuronal and epithelial cells of embryonic eye tissues in both mice and humans. However, the mechanisms by which either Mid or Tbx20 function to regulate cell-fate specification or other critical aspects of eye development including cell survival have not yet been elucidated. We have also gathered preliminary evidence suggesting that Mid may play an indirect, but vital role in selecting SOP cells within the third-instar larval eye disc by regulating the expression of the proneural gene *atonal*. During subsequent pupal stages, Mid specifies SOP cell fates as a member of the Notch–Delta signaling hierarchy and is essential for maintaining cell viability within by inhibiting apoptotic pathways. We present several new hypotheses that seek to understand the role of Mid in regulating developmental processes downstream of the Notch receptor that are critical for specifying unique cell fates, patterning the adult eye and maintaining cellular homeostasis during eye disc morphogenesis.

* Corresponding author. Address: University of Southern Mississippi (USM), Department of Biological Sciences, 118 College Drive 5018, Hattiesburg, MS 39406, United States. Tel.: +1 6012666050; fax: +1 6012665797. sandra.leal@usm.edu, Igfbp3@aol.com (S.M. Leal).

5. Uncited references
Heitzler et al. (1996), Romain et al. (1993), and Schweisguth (2004).

Appendix A. Supplementary data

Supplementary data associated with this article can be found, in the online version, at <http://dx.doi.org/10.1016/j.mod.2013.08.001>.

Keywords

Midline; Tbx20; Notch; Delta; Extramacrochaetae; Atonal; Senseless; Sensory Organ Precursor Cell; Baculovirus p35; Apoptosis

1. Introduction

1.1. Midline, Tbx20 and eye development

We initiated a study examining the role of the T-box transcription factor gene *midline* (*mid*) in regulating *Drosophila* eye development. The *Tbx20* gene is the vertebrate homolog of *mid* and in the mouse visual system *Tbx20* transcripts are expressed in the periphery of the neural retina and within the optic cup of early-staged fetuses (Meins et al., 2000). In late-staged fetuses, *Tbx20* mRNA is detected in the neural retina, pigment epithelium, optic nerve and sclera and by 13 weeks of gestation, is broadly detected in the sclera, optic nerve and cornea as well as both the ganglion and neuroblastic layers of the neural retina (Meins et al., 2000; Kraus et al., 2001). While this research implicates the importance of *Tbx20* in regulating the development of diverse cell types within the eye, the Tbx20- and Mid-regulated TF networks that guide cell-fate specification and tissue morphogenesis within developing eye tissues are largely unknown.

The *Drosophila* compound eye is an excellent model system for genetically dissecting *mid* TF regulatory networks. Several evolutionarily conserved signaling pathways have been identified in which structurally unique TFs regulate gene expression to specify cell fates and to guide pattern formation during eye development including the Notch–Delta and transforming growth factor-*beta* (TGF- β) signaling pathways (Tripathi et al., 1991; Silver and Rebay, 2005; Doroquez and Rebay, 2006; Lovicu et al., 2011). We present studies that showcase the multifaceted developmental roles of *mid* as a gene regulating neuronal cell fate specification, cellular survival and tissue patterning of the eye disc in the context of the Notch–Delta signaling pathway. We also present preliminary results suggesting that a co-regulatory relationship may exist between Mid and TGF- β signaling pathways essential for proper eye development.

1.2. *Drosophila* eye development

The *Drosophila* eye is comprised of ~700–750 unit facets organized in an array first described as a “neurocrystalline lattice” (Ready et al., 1976; reviews by Kumar, 2012; Tsachaki and Sprecher, 2012). A single facet, or ommatidium, consists of several distinct cell types arranged in a pattern that is precisely reiterated among all ommatidia. A cluster of eight photoreceptor neurons (PNs) designated as R1–R8 PNs are flanked by a primary pigment cell on either side. Four lens-secreting cone cells are positioned above the PNs completing a unit core (Tomlinson and Ready, 1987). Six secondary and three primary pigment cells surround this core in a hexagonal shape and are shared among ommatidia. An interommatidial bristle (IOB) complex is located within each of three alternate vertices between tertiary pigment cells with a total of ~400 IOBs spanning the compound eye. An IOB complex consists of a shaft cell, socket cell, sheath cell and sensory neuron (Wigglesworth, 1953; Waddington and Perry, 1960).

Eye development is initiated from a monolayer of epithelial cells in the central-posterior margin of the third-instar (3[°]L) imaginal eye disc. Within this domain, Decapentaplegic (Dpp), a homolog of the vertebrate TGF- β ligand (Heberlein et al., 1993), activates the expression of early retinal determination transcription factors (TFs) regulating gene expression essential for initiating the formation of the morphogenetic furrow (MF), a band of epithelial cells that undergoes a passing apical to basal contraction from the posterior to anterior regions (Fig. 12A) (Silver and Rebay, 2005). As the MF progresses anteriorly, a sequential recruitment of single or paired PNs from a pool of equivalent cells occurs in the following order: R8, R2/R5, R3/R4, R1/R6 and R7 (reviewed by Wolff and Ready, 1993). The specification and temporal-spatial assembly of the first R8 through the final R7 PN within each cluster depends upon the activation of Notch–Delta and epidermal growth factor receptor (EGFR) signaling pathways as well as cell–cell contacts among recruited PNs (Cagan and Ready, 1989a; Freeman, 1996, 1997). Missteps in the specification or assembly of PNs result in severe ommatidial patterning defects (Pickup et al., 2002).

1.3. R8. photoreceptor neurons are selected from a proneural field of equivalent cells

R8 PNs are selected from proneural fields of neuronally competent cells that express Atonal (Ato), a basic helix-loop-helix (bHLH) TF protein marking ~10–15-cell clusters referred to as intermediate groups (IGs) (Fig. 12A) (reviewed by Frankfort and Mardon, 2002; Jarman et al., 1994, 1995; Freeman, 1997). Dpp regulates a narrow dorsal–ventral band of Ato expression anterior of the MF. This band of cells generates IGs within the MF that secrete Scabrous (Sca), a glycoprotein and Notch receptor ligand. Sca establishes local inhibitory gradients to maintain regular spacing among IGs (Baker and Zitron, 1995). Approximately 2–3 Ato-expressing cells from each IG migrate from the basal to apical plane of the MF as an R8 equivalence group (Fig. 12A) (Dokucu et al., 1996). Cells of the equivalence group transiently co-express Ato and Senseless (Sens), a proneural zinc-finger TF protein. Subsequently, *ato* expression is inhibited by the homeodomain TF Rough (Ro) in all cells of the equivalence group except for the selected pre-R8 cell (Dokucu et al., 1996; Pepple et al., 2008). During the pre-R8 to R8 transition, Ato continues to activate *sens* expression before succumbing to negative inhibition mediated by both Ro and Notch (Pepple et al., 2008). Emergent R8 PNs linearize along column 1 posterior of the MF and become terminally specified within column 4 (Pepple et al., 2008).

1.4. The specification of R8 photoreceptor neurons is regulated by a Notch–Delta lateral inhibition mechanism

Pre-R8 cells inherently express higher levels of the Notch receptor ligand Delta than surrounding cells and are designated as Delta-sending cells (Cubas et al., 1991; Skeath and Carroll, 1991; Parody and Muskavitch, 1993; Muskavitch, 1994; Parks et al., 1995). The Delta-activated Notch receptor initiates a lateral inhibition mechanism in juxtaposed Delta-receiving cells (Ligoxygakis et al., 1998); both Notch and Delta are transmembrane proteins (Fig. 12B). The pre-R8 cell also secretes Sca to enhance Notch activity in response to Delta (Lee et al., 1996; Mok et al., 2005) inducing a conformational change in Notch and the proteolytic cleavage of the Notch intracellular domain (Notch_{ICD}) (Schroeter et al., 1998; DeStrooper et al., 1999). The Notch_{ICD} translocates into the nucleus and associates with Suppressor of Hairless [Su(H)], converting Su(H) from an inhibitor to a co-transcriptional

activator of the *Enhancer of Split [E(Spl)]* gene complex (Artavanis-Tsakonas et al., 1995; Ligoxygakis et al., 1998). The E(Spl) TF proteins inhibit the expression of proneural gene targets including *ato*, *sens* and *daughterless (da)* and commit these cells to assume default, non-neuronal fates (Fig. 12B).

E(Spl) proteins functioning within Notch lateral inhibition pathways are predicted to interact with extramacrochaetae (Emc) and have been shown to inhibit proneural gene expression during wing disc development (Baonza et al., 2000). Emc is a helix-loop-helix (HLH) TF lacking a basic DNA binding domain that sequesters Daughterless (Da), a proneural gene, from DNA binding sites via heterodimer formation (Ellis et al., 1990; Garrell and Modolell, 1990; van Doren et al., 1991; Cadigan and Nusse, 1996; Smith and Cronmiller, 2001; Cadigan et al., 2002; Bhattacharya and Baker, 2011). Since Da heterodimerizes with Ato (Jarman et al., 1993), Emc also indirectly impacts Ato binding activity. By delimiting Da and Ato binding to specific DNA binding sites of proneural target genes, Emc further consolidates the non-neuronal cell fate. Conversely, within Delta-sending cells, Emc activity is either inhibited by specific E(spl) proteins or other unknown interactors downstream of Notch allowing Ato and Da to activate *sens* gene expression (Baonza and Garcia-Bellido, 1999).

1.5. The SOP cell acquires a neuronal fate specified by a Notch–Delta lateral inhibition mechanism and gives rise to the interommatidial bristle cell lineage

SOP cells are specified asynchronously 0–6 h after puparium formation (APF) and become designated as ganglion mother cells (GMCs). The specification of SOP cells in the imaginal eye disc does not require EGFR signaling, but utilizes the conserved TF network of the Notch signaling pathway specifying PN fates (Fig. 12B). In addition to *da* and *sens*, however, SOP cells activate proneural genes of the *achaete–scute complex (ASC)* (Frankfort et al., 2004). Unique from PN assembly, GMCs in the eye disc establish a cell lineage via a series of asymmetric divisions. Each GMC divides to generate a PIIa and PIIb daughter cell. The PIIa cell, in turn, divides giving rise to a socket and shaft cell (Fig. 12C1) while the PIIb division generates a PIIIb daughter cell and terminal glial cell. The PIIIb divides into a sheath and sensory neuron (Cagan and Ready, 1989a). The specification of daughter cells in the GMC lineage produced from asymmetric divisions is regulated by Notch and Numb (Nb), a Notch antagonist (Fig. 12C1) (Guo et al., 1996; Rebeiz et al., 2011).

1.6. Programmed cell death refines the retinal pattern of the compound eye and is also regulated by Notch signaling

During the specification of SOP cells, excess interommatidial precursor cells are eliminated by Notch-induced apoptosis to maintain precise ommatidial spacing (Cagan and Ready, 1989b; Hay et al., 1994; Go et al., 1998; Miller and Cagan, 1988; Yu et al., 2002; Copeland et al., 2007; Koto et al., 2011). Apoptosis of neuronal precursors during eye development is specifically regulated by the *Drosophila* homolog of the vertebrate tumor suppressor p53 (dp53) (Dichtel-Danjoy et al., 2013) following the activation of the pro-apoptotic genes *grim* (Chen et al., 1996), *reaper (rpr)* (White et al., 1994) and *head involution defective (hid)* (Grether et al., 1995). In addition, Emc, Sens and Ato have been linked to regulating cell proliferation and cell death signaling pathways in the developing eye and other organ

systems of *Drosophila* (Baonza and Garcia-Bellido, 1999; Chandrasekaran and Beckendorf, 2003; Adam and Montell, 2004; Bossuyt et al., 2009;). We present new evidence that *mid* collaborates with *emc*, *ato* and *sens* downstream of Notch not only to specify SOP cells, but also to maintain cellular homeostasis among PNs while unessential cells are removed by apoptosis.

2. Results

2.1. *mid* Loss-of-function mutations generated within the eye epithelial disc result in a significant loss of interommatidial bristles

Using the *glass multiple reporter (GMR) Gal4* driver line (Hay et al., 1994) and previously characterized *UAS-mid-RNAi* trans-genes (Qian et al., 2005; Leal et al., 2009), we generated a perpetual stock of transgenic flies to specifically reduce *mid* expression within cells posterior of the MF during 3°L and early pupal stages of eye imaginal disc development (Brand and Perrimon, 1993). We closely examined the phenotype of compound eyes from wild-type (WT) and *UAS-mid-RNAi/CyO; GMR-Gal4/TM3 (mid-RNAi)* 1-day old adult female flies with high-resolution scanning electron microscopy (SEM). Compared to WT eyes, *mid-RNAi* mutant eyes exhibited a composite of multiple overlapping tissue defects including decreased bristle numbers, bristle polarity defects, bristle shaft deformations, empty socket cells, abnormally paired bristle complexes and extensive ommatidial fusion (Fig. 1A and B). We obtained ten SEM images of WT and *mid-RNAi* adult compound eyes and counted interommatidial bristles to accurately detect an approximate 50% decrease of bristles across the entire eye field of *mid-RNAi* mutants. We observed a significant reduction of bristles within the ventral region compared to the dorsal region of the eye field (Fig. 1C) and also compared bristle numbers in the posterior and anterior regions (Fig. 1D).

The mutant bristle phenotype of the whole eye field provided an ideal sensitized *mid* loss-of-function (LOF) phenotype in which to undertake a genetic modifier screen by crossing third chromosomal deficiency lines from the *DrosDel* collection to *mid-RNAi* flies and determining whether the *mid-RNAi* mutant phenotype was enhanced or suppressed. To increase the efficiency of the screen, we repeated these studies using a high-magnification light microscope to capture and record 10 montaged images of WT and *mid-RNAi* mutant eyes (see Methods). By digitally tagging and counting IOBs from these images, we determined that *mid-RNAi* mutant eyes exhibited an approximate 49% decrease of interommatidial bristles compared to WT eyes although we lost a minor degree of resolution in the detection of ventral bristles due to lighting conditions and eye curvature (Fig. 1E–H). Despite a small offset in numbers, the mean reduction in bristle numbers of *mid-RNAi* eyes normalized as a percentage of the mean bristle numbers of WT eyes was approximately 50% using either SEM or montaged images from the light microscope to quantify them.

In addition to bristle loss and disorganized ommatidia, the light microscope images revealed decreased pigmentation due to either the loss or misspecification of one or more 1°, 2° and 3° pigment cells (Fig. 1F and G). We crossed several *UAS-mid-RNAi* transgenic flies to the *54C-Gal4* driver line that targets *mid* reduction in pigment cells (Nagaraj and Banerjee, 2007) and observed no changes in their development or pigmentation suggesting that under *mid-RNAi* conditions utilizing the *GMR-Gal4* driver, these cells may have been collaterally

perturbed in a cell non-autonomous manner (data not shown). In approximately 20% of the *mid-RNAi* flies screened, reduced *mid* expression resulted in patches of melanized tissue indicative of apoptotic or necrotic cell death as well as some tissue scarring in the eye (Fig. 1G). In all studies, mutant *mid-RNAi* eyes exhibiting any degree of scarring were excluded from quantitative and statistical analyses of bristle numbers.

To confirm that the *mid* mutant phenotype induced by the *UAS-Gal4* system and RNAi method was specific, we assayed the individual effects of heterozygous transgenes for *UAS-mid-RNAi* or *GMR-Gal4* and bristle numbers were normal compared to Oregon-R (OR) WT fly eyes (Supplementary Fig. S1). We also validated these effects by crossing other transgenes for *UAS-mid-RNAi* with a *GMR-Gal4* driver on the second chromosome (data not shown). We then generated mosaic clones null for both *H15* and *mid* (*H15/mid*) and examined the eyes of 1-day old flies using SEM. The *H15* T-box gene paralog was previously shown to function in a partially redundant manner with *mid* to regulate heart and neuronal cell fate specification as well as to pattern the epidermis (Qian et al., 2005; Buescher et al., 2004, 2006; Leal et al., 2009). We detected a nearly complete loss of bristles within *H15/mid* null tissues of the compound eye characterized by widespread ommatidial fusion that recapitulated the *mid-RNAi* mutant phenotype (Fig. 2C).

The disrupted *H15/mid* mutant eye tissue also partially phenocopied a Notch (*N^{full}*) gain-of-function (GOF) mutation suggesting a possible link to the Notch–Delta pathway specifying SOP cell fates (Fig. 2D) (Hagedorn et al., 2006). We then crossed *UAS-mid-RNAi* flies to a transgenic line carrying both *scabrous (sca)-Gal4* and *prospero (pros)-Gal4* that target the expression of Gal4 in proneural SOP cells and their PIIb daughter cells, respectively (Nakao and Campos-Ortega, 1996; Shiga et al., 1996). Under these conditions, we detected an expansion of ommatidial columns within the posterior domain of the eye field lacking IOBs (Fig. 2F). In a few rows of ommatidia, we observed an 180° shift in the orientation of bristles suggestive of polarity defects (Fig. 2F, inset).

2.2. A *mid* gain-of-function phenotype results in ommatidial patterning defects

Generating *mid* gain-of-function (GOF) mutants using the *GMR-Gal4* driver and the *UAS-Gal4* system resulted in an excess of small, trichome-like shaft cells in the dorsal region of the adult eye (Fig. 3C). The data show that overexpressing *mid* results in a phenocopy of a *Notch* loss-of-function (LOF) mutation at the level of the PIIa cell. Misspecification of PIIa precursor cells under *Notch* LOF conditions has been previously shown to give rise to small bristle shafts without sockets (Lai and Orgogozo, 2004). Since a *mid* GOF mutation resulted in severe eye developmental defects similar to *mid* LOF mutations including loss of bristles, bristle defects and ommatidial fusion (Fig. 3B and C), attempts to rescue the *UAS-mid-RNAi* mutant phenotype by overexpressing *mid* in the *mid-RNAi* background with a range of *UAS-mid* constructs were not effective (data not shown). Of the *UAS-mid* transgenes assayed, one provided a dosage of *mid* expression that, albeit incomplete, partially rescued bristle numbers to normal levels observed in WT flies (Supplementary Fig. S2).

Overexpressing *H15* in the *mid-RNAi* background resulted in pupal lethality suggesting that high levels of H15 are as functionally pervasive, if not more so, than increased levels of Mid. On the one hand, this result agrees partly with the functional redundancy of *H15* with

mid to effect cell-fate specification under specific GOF conditions (Qian et al., 2005). On the other hand, all reported *H15* LOF experimental conditions indicate that *H15* is not an essential gene mediating cell-fate specification in WT developing tissues including the heart, CNS and epidermis (Qian et al., 2005; Buescher et al., 2004, 2006; Leal et al., 2009). Flies homozygous mutant for null alleles of *H15* are viable and exhibit normal eyes and bristle numbers although visual acuity has not been examined (data not shown). Examining *H15* null clones using mosaic analyses was prohibitive since the *H15* and *mid* genes are located within close proximity to each other.

2.3. Mid and H15 are expressed within photoreceptor neurons and SOP cells of the eye imaginal disc

Before proceeding further, we examined the co-expression pattern of Mid and H15 in specific cell types across early stages of eye disc development in greater detail. Beginning in the 3^oL stage, we first detected both Mid and H15 in R1–R8 PNs marked by the expression of Elav, a neural-specific, RNA binding protein required for the proper development of neurons within the developing CNS and visual system (Fig. 4A–D) (Yao et al., 1993). Mid and H15 are expressed in all PNs in a pattern that overlaps with Elav (Fig. 4A–D). At 0–3 h after puparium formation (APF) during the P1–P2 stages, we detected H15 and Mid within PN clusters also marked by Elav (Fig. 5A–D). At 3–6 h APF at the P3 stage when a majority of SOP cells are specified (Frankfort et al., 2004), we observed a dramatic shift in the expression pattern of Mid and H15 with respect to Elav. Mid and H15 were co-expressed in a small population of photoreceptor neuron clusters marked by Elav and within a minor population of SOP cells distinguished by linear arrays of single cells expressing Mid and H15, but lacking Elav expression (Fig. 5G and H).

To confirm SOP cell identities directly, we co-immunolabeled P3 staged WT pupal eye discs with anti-Mid antibody and a specific antibody to detect Ac, an SOP cell marker. Mid and Ac expression overlapped within a majority of SOP cells (Fig. 6A–C). We then examined the expression pattern of Ac in P3-staged *mid-RNAi* eye discs. Reduced *mid* expression resulted in a significant decrease of Ac within SOP cells (Fig. 6D–F). We also generated numerous small mitotic clones null for *H15/mid* throughout a P3-staged eye disc and found that most, if not all clones, lacked Ac expression except for a minor band that formed within the MF (Fig. 6G–I). We validated these results using a different antibody that marks the SOP cell, anti-Sens. Sens and Mid were co-expressed in SOP cells (Fig. 6J–L). As observed for Ac, Sens expression was dramatically reduced within *mid-RNAi* discs (Fig. 6M–O). However, we did not detect any changes in Sens expression within either small or large mitotic clones null for *mid/H15* generated within P3-staged discs posterior of the MF (data not shown).

2.4. Mid antagonizes Emc activity to regulate interommatidial bristle complex formation

We gathered preliminary data suggesting that *mid* functions within the Notch–Delta signaling pathway specifying SOP cell fates. We also uncovered a chromosomal deficiency, *Df(3L)ED207*, that when placed in a heterozygous state within the *mid-RNAi* background significantly suppressed the *mid* mutant phenotype and recovered bristles (data not shown). Overlapping chromosomal deficiency analyses delimited one cytological interval within

Df(3L)ED207 harboring potential *mid*-interacting genes to the 61C8-61D2 region (see Methods; data not shown). Surveying the identity of 60 genes deleted from this interval, we concluded that the *emc* gene was a *mid*-collaborating gene of high interest since it was previously shown to specify SOP cell fates downstream of the Notch receptor (Flybase.org) (Ellis et al., 1990). However, we cannot rule out the possibility that remaining gene candidates deleted from the interval interact with *mid*. Studies are in progress to complete the chromosomal overlapping deficiency analyses and to screen mutant alleles of potential *mid*-interacting gene candidates.

Generating *UAS-mid-RNAi/+;GMR-Gal4/emc¹* flies, we found that removing one functional copy of the *emc* gene in the *mid-RNAi* background significantly suppressed the *mid-RNAi* phenotype; *emc¹* is a null allele (Fig. 7E and I). A high-resolution SEM image of a *UAS-mid-RNAi/CyO; GMR-Gal4/emc¹* eye details the significant recovery of bristles by ~25% and relatively normal ommatidial structures (Fig. 7H). These results implicate a cell-survival role for Mid as an antagonist of Emc function. Because the only available anti-Mid and anti-Emc antibodies were raised in the same species, we co-immunolabeled P2-staged WT and *mid-RNAi* pupal discs with anti-H15 and anti-Emc antibodies. The anti-H15 is a faithful surrogate reporter for Mid expression as both H15 and Mid expression overlapped in both PNs (Fig. 4) and SOP cells (Fig. 5). H15 and Emc were co-expressed in 3°L eye discs (Supplementary Fig. S3). We did not detect a significant difference in Emc expression levels between WT or *mid-RNAi* discs posterior of the MF. Changes in the tissue integrity anterior of the MF made it difficult to assess whether Emc accumulated within this region (Supplementary Fig. S3).

2.5. *mid* regulates the expression of Delta and Scabrous within the MF

We undertook a wide range of co-expression analyses of Mid in WT and stage-matched *mid-RNAi* 3°L eye discs with antibody probes specific for identifying cellular structures, Notch pathway signaling proteins and unique cell types (Supplementary Table S1). These studies indicated that *mid* does not regulate the specification of PNs, glial cells or cone cells. Reducing *mid* expression also did not affect the assembly, spacing or adhesion properties of PN clusters posterior of the MF. Under *mid-RNAi* conditions, however, we detected a minor reduction of Delta expression (Fig. 8D–F) and a complete loss of Sca expression (Fig. 8M–O) within the MF. We generated *H15/mid* LOF clones within 3°L eye discs and compared the expression pattern of Delta and Sca within mutant and surrounding WT tissue. We noticed that large *H15/mid* null clones generated within the MF that clipped both the anterior and posterior flanking tissue exhibited reductions in Delta expression (Fig. 8G–I) and a complete loss of Sca expression (Fig. 8P–R).

Recently, *cis*-regulatory modules for Tbx16 were identified upstream of the Zebrafish *delta-c* gene (Jahangiri et al., 2012). Based upon new evidence linking vertebrate T-box TF activity to the regulated expression of a *delta* homolog and from the analyses of data we gathered from the *mid-RNAi* eye phenotype and *H15/mid* LOF studies detecting reductions in the expression of Delta and Sca, we sought to resolve whether *mid* functions downstream of *Notch-Delta* to regulate SOP cell fate specification. The identification of *emc* as a *mid*-

collaborating gene further catalyzed genetic studies to place *mid* within the *Notch–Delta* genetic hierarchy specifying SOP cell fates.

2.6. Genetic studies place *mid* within the *Notch–Delta* pathway specifying SOP cell fates

We undertook allelic genetic modifier studies by placing *mid-RNAi* flies within heterozygous null mutant backgrounds of genes known to function within the *Notch–Delta* genetic pathway including *Su(H)*, *E(spl)-m8*, *H*, *hairy (h)*, *atonal (ato)*, *da*, *ac*, *sc*, and *sens*. Although not absolutely required for eye development, the *h* gene functions as a repressor of proneural gene expression in the PNS (Brown et al., 1991; Ohsako et al., 1994; van Doren et al., 1991). We assayed the *h¹* mutant as a negative control to test the fidelity of the allelic modifier screen. As expected, a range of heterozygous mutant alleles of *Notch*, *Delta*, *da* and the *ac–sc* complex exhibited a significant loss of IOBs and could not be assayed. However, *Su(H)¹*, *E(spl)-m8-HLH¹*, *H¹*, *h¹*, *ato¹*, *da¹*, *ac¹* and *sens^{E2}* heterozygous LOF mutant alleles exhibited normal bristle numbers compared to WT flies and were each independently crossed to *mid-RNAi* flies.

For several combinations of heterozygous mutant alleles placed in the *mid-RNAi* background, we observed that the *GMR-Gal4* driver line contributed to an ~10–25% decrease in bristles (Figs. 7, 9 and 10, Supplementary Fig. S4). Eyes examined of the genotype *+/H¹;GMR-Gal4/TM3* exhibited the most significant decrease of bristles by ~25% (Supplementary Fig. S4). Since *UAS-mid-RNAi/H¹;GMR-Gal4/TM3* flies also exhibited an ~25% reduction of bristles, we negated a modification of the *mid* mutant phenotype by a heterozygous mutant allele of *H¹* and retained *H* within the genetic pathway (Fig. 12B). The contribution of the *GMR-Gal4* transgene to bristle loss may result from at least two biological possibilities. The *GMR-Gal4* transgene insertion site may be disrupting an enhancer region that regulates the expression of one or more genes essential for bristle formation or cell viability. Alternatively, the Gal4 TF may be activating endogenous enhancer regions independently of the UAS target site as reported recently for wing disc development (Li et al., 2012). The non-specific Gal4 effects did not significantly impact the results or interpretation of the allelic genetic modifier study. The suppression levels we quantified for mutant alleles are conservative estimates of bristle recovery. By removing one copy of each mutant allele screened, dosage effects in the allelic genetic modifier assay are half-maximal. In theory, null allelic mutations would result in a greater suppression of IOB generation.

Of the mutant heterozygous alleles assayed, the proneural genes *ato¹* (Fig. 9E and H–J) and *sens^{E2}* (Fig. 10E and H–J) significantly suppressed the *mid-RNAi* bristle phenotype. Placing *E(spl)-m8-HLH¹*, *Su(H)¹*, *H¹*, *h¹*, *da¹* or *ac¹* heterozygous mutant alleles within the *mid-RNAi* background did not modify the mutant phenotype (Supplementary Table S1). Given the dosage constraints of the modifier assay, these latter results may represent false negatives. For example, using immunolabeling methods, Ac expression was significantly reduced within SOP cells of *mid-RNAi* pupal discs (Fig. 6D–F). As supported by the combined expression and genetic analyses as well as numerous published studies that genetically confirm a *Notch* signaling pathway (see Introduction) (Fig. 12B), we have placed *mid* upstream of *E(spl)* and *emc*, in parallel with *Su(H)* and *H* and epistatic to the *Notch–*

Delta lateral inhibition pathway specifying SOP cell fates. The *da*, *ac*, *ato* and *sens* proneural genes are placed downstream of *emc* (Fig. 12B).

2.7. Placing a heterozygous mutant allele of *atonal* in the *mid*-RNAi background expands the proneural fields giving rise to R8 and SOP precursor cells

We predicted that decreasing *ato* expression in the *mid*-RNAi background would enhance the mutant bristle pheno-type and result in greater bristle loss. Paradoxically, we observed the contrary result. The mutant bristle phenotype was suppressed. To understand how reducing *ato* expression in the *mid*-RNAi background recovered bristles, we immuno-stained *UAS-mid*-RNAi/+; *ato*¹/*GMR-Gal4* 3°L imaginal eye discs with either anti-Ato or anti-Sens antibodies. Compared to WT and *ato*¹ heterozygous eye discs (Fig. 9K and L), *UAS-mid*-RNAi/+; *ato*¹/*GMR-Gal4* discs lacked Ato-expressing R8 equivalent cells emerging from the MF and Ato-expressing IGs were not clearly demarcated (Fig. 9N). Despite these major changes in Ato expression, the specification of R8 PNs was unaffected. Sens marked R8 PNs within *UAS-mid*-RNAi/+; *ato*¹/*GMR-Gal4* eye discs (data not shown). We also detected a diffuse gradient of Ato expansion either within or anterior of the furrow that is divided by a band of unlabeled cells resembling a groove across and in *UAS-mid*-RNAi/+; *ato*¹/*GMR-Gal4*. Further immunolabeling studies with specific markers to detect the MF will resolve the localization pattern of Ato under *mid*-RNAi mutant conditions including those carrying heterozygous null mutant alleles.

2.8. Reducing *mid* expression induces apoptosis within early pupal stages

Due to aberrant Notch–Delta signaling, we predicted that *mid*-RNAi pupal discs would exhibit abnormally high numbers of incorrectly specified epithelial cells generated at the expense of SOP cells. Therefore it was plausible that excess epithelial and interommatidial precursor cells were likely undergoing apoptosis on a much larger scale than basally required for patterning the WT eye (Wolff and Ready, 1991). To determine whether apoptosis contributed to decreased formation of IOBs and other cell types, we generated flies of the genotype *UAS-p35*/*w*¹¹¹⁸; *UAS-mid*-RNAi/+; *GMR-Gal4*/+ overexpressing a baculoviral anti-apoptotic gene *p35* in the *mid*-RNAi background (LaCount et al., 2000). Overexpressing *p35* partially suppressed the *mid*-RNAi mutant bristle phenotype (Fig. 11D–F). Although bristles showed a slight degree of disorientation within the center of the eye, a majority of bristle complexes were recovered radially in an outward to inward pattern (Fig. 11D). The radial generation of eye bristles in WT flies has been previously described (Cagan and Ready, 1989b).

The recovery of bristles and cell viability of ommatidia by *p35* indicates that bristle loss in *mid*-RNAi eyes results in part from apoptosis. We further examined *mid*-RNAi pupal eye discs during the P3 stage of development for cell death with the apoptotic marker Caspase-3 and DAPI to examine nuclear morphology. We detected increased Caspase3 expression levels in *mid*-RNAi discs compared to WT discs (Fig. 11H). DAPI labeling identified proapoptotic bodies and tissue disintegration (Fig. 11H'). In addition, placing the *mid*-RNAi background in a heterozygous *Df(3L)H99* background deficient of the proapoptotic genes *grim*, *reaper* and *hid*, partially suppressed the *mid* mutation (White et al., 1994) (Fig. 11I–M). Based upon these comprehensive studies, we conclude that IOB loss in *mid*-RNAi

tissues results from misspecification and the induction of abnormally rampant apoptosis. Future studies to decipher *mid* function as a cell-fate determinant and pro-survival factor will dissect specific cell signaling pathways genetically on a “gene by gene” basis and within narrower windows of eye imaginal disc development.

3. Discussion

3.1. Mid functions within the Notch–Delta genetic pathways regulating the specification of SOP cells into ganglion mother cells during early pupation

The specific developmental stage and duration in which Notch signaling is disrupted can affect one or more eye developmental processes including the specification, arrangement or survival of photoreceptor neurons, accessory cells, SOP cells and/or daughter cells of the SOP-cell lineage. Inducing a temperature-sensitive GOF *Notch* transgene encoding the *Notch* intracellular domain (*Notch^{int}*) 0–16 h after puparium formation (APF) was previously shown to suppress SOP cell generation while the development of ommatidia was largely undisturbed (Lyman and Yedvobnick, 1995). Overexpressing the full-length *Notch* (*N^{Full}*) receptor using the *GMR-Gal4* driver more closely resembled the *mid-RNAi* phenotype than the reported temporal induction of *Notch^{int}* (Fig. 2D) (Lyman and Yedvobnick, 1995; Go et al., 1998; Hagedorn et al., 2006). The *GMR* enhancer-promoter drives expression within and posterior of the MF beginning in the 3°L stage. The promoter remains active for 60 h APF and drives expression in all retinal cells except for cone cells (Moses et al., 1989; Ellis et al., 1993). During the developmental window in which we targeted *mid* transcript degradation via RNAi using the *UAS-mid-RNAi* and *GMR-Gal4* drivers, we detected not only widespread IOB loss, but also cellular degeneration and fused ommatidia (Fig. 1A and B).

The similarity of the *N^{Full}* and *mid-RNAi* mutant phenotypes led us to hypothesize that *mid* functions within the *Notch–Delta* pathway regulating SOP cell fate specification and cell survival. As mentioned, Mid is expressed in all accessory pigment cells. However, reducing *mid* transcript expression did not affect the pigmentation or morphology of these cells (data not shown). Mid is also expressed in differentiating PNs during later pupal stages (data not shown) and efforts are underway to determine whether Mid regulates the morphogenesis of rhabdomeres (Mollereau and Domingos, 2005) or other terminal aspects of specific PN differentiation including the outgrowth of axons that establish synaptic connections with the lamina (R1–R6) and medulla (R7, R8) of the optic lobe (Cutforth and Gaul, 1997). We are confident, however, that Mid is not essential for PN specification (Supplementary Table S2). Immunolabeling R1–R8 PNs of *mid-RNAi* discs with a range of specific PN markers including anti-Elav, anti-Lozenge and anti-Boss antibodies indicated that the generation and arrangement of PNs under *mid-RNAi* conditions and within *H15/mid* null mitotic clones were normal (Supplementary Table S2).

Confirming that *mid* functions downstream of *Notch–Delta* to specify SOP cell fates, we detected a significant decrease of Ac and Sens expression in a majority of SOP cells within *mid-RNAi* pupal discs 6 h APF as compared to stage-matched WT eye discs (Fig. 6). By undertaking the genetic modifier studies on the *mid* LOF mutation using a range of mutant alleles within the Notch–Delta signaling pathway, we placed *mid* downstream of *Notch–*

Delta, upstream of both *emc* and *E(spl)* and in parallel with *Su(H)* and *H* in both SOP and epidermal cells (Fig. 12A) (Baonza et al., 2000). As depicted in the genetic schemes supported by nearly two decades of cumulative research, Mid antagonizes Emc in the Delta-signaling cell (Fig. 12A) (see all references cited in Sections “The SOP cell acquires a neuronal fate specified by a Notch–Delta lateral inhibition mechanism and gives rise to the interommatidial bristle cell lineage” and “Programmed cell death refines the retinal pattern of the compound eye and is also regulated by Notch signaling”). As a result, Emc cannot sequester Da leading to Da-activated *sens* expression and the final conversion of the SOP cell to the neuronal GMC or bristle mother cell fate (Jafar-Nejad et al., 2003; Frankfort et al., 2004; Bao, 2010). Conversely, in Delta-receiving cells, in which the cleaved Notch_{ICD} translocates into the nucleus, neither Mid and/or E(Spl) TFs negatively impact Emc activity. Emc sequesters Da and silences proneural gene expression to consolidate the default epidermal cell fate (Fig. 12A).

3.2. mid functions as a pro-survival factor in developing pupal discs

We detected increased apoptosis in *mid-RNAi* flies that was partially suppressed by overexpressing the caspase inhibitor p35 (Fig. 11D) or by removing one copy of the pro-apoptotic genes *grim*, *rpr* and *hid* in a *Df(3L)H99* background (Fig. 11I–M). Since reduced *mid* expression appeared to generate epidermal cells at the expense of SOP cells (Fig. 12B2), an expansion of epidermal cells in *mid-RNAi* discs may have triggered the preemptive warning signal amplifying the apoptotic response above basal levels. Due widespread apoptosis, we speculated that the organization of surviving accessory cells was disturbed as the cellular landscape changed. As discussed, missteps in the arrangement of cells during any stage of eye development lead to severe patterning defects (Pickup et al., 2002).

Interestingly, in a reported genetic modifier screen of a *H* GOF apoptotic mutant phenotype with degenerative features similar to the *mid-RNAi* phenotype, *emc* was not identified as an enhancer or suppressor of *H* (Muller et al., 2005). Thus, it follows that *emc* does not function within a *Notch* LOF genetic pathway as the screen by Muller et al. (2005) determined. Rather, our studies suggest that under permissive Notch signaling when levels of *mid* are reduced experimentally via RNAi, Emc activity is increased as a GOF effect resulting in fewer specified SOP cells and subsequent apoptosis (Fig. 12A). Muller et al. (2005) also reported that placing a heterozygous *Df(2L)sc19-4* chromosomal deficiency within the *GMR-Gal4/+;UAS-H/CyO* background led to an enhancement of the apoptotic phenotype. Since *mid* and *H15* are deleted from this interval, the screen confirms the potential of *H15/mid* to function as pro-survival factors. The *thickveins (tkv)* gene, a TGF- β type I receptor, was also deleted from *Df(2L)sc19-4* and represents an additional pro-survival candidate gene with potential ties to *mid* function during eye development as discussed in Section “Does Mid function in a cell non-autonomous manner to select pre-SOP cells during the 3oL stage of eye imaginal disc development?” (Affolter et al., 1994).

Other TF regulatory networks in which *mid* functions to regulate cell survival warrant further study and are likely to converge on *Drosophila p53 (dp53)*, a *Drosophila* homolog of the mammalian tumor suppressor gene *p53* (reviewed by Rutkowski et al., 2010). Effector

caspsases downstream of *dp53* have been shown to reduce cellular proliferation rates providing evidence of a link between apoptotic and oncogenic pathways in *Drosophila* (Mesquita et al., 2010). Moreover, overexpressing human *p53* in the developing *Drosophila* eye imaginal disc induces severe apoptosis (Yamaguchi et al., 1999). The uncovered function of *mid* as a pro-survival gene will provide a foundation for comparative functional studies of *Tbx20* within vertebrates since deregulated apoptotic signals are associated with the development of cancer and neurodegenerative diseases including retinoblastoma in which *p53* is inactivated (Vuong et al., 2012).

3.3. Does *Mid* function in a cell non-autonomous manner to select pre-SOP cells during the 3°L stage of eye imaginal disc development?

While the recovery of bristles observed in *UAS-mid-RNAi/+;GMR-Gal4/emc¹* eyes was a logical result based upon the placement of *mid* within the *Notch–Delta* genetic hierarchy specifying SOP cell fates (Figs. 7 and 12A), the significant recovery of bristles detected in *UAS-mid-RNAi/+;GMR-Gal4/ato¹* (Fig. 9) and *UAS-mid-RNAi/+;GMR-Gal4/sens^{E2}* eyes (Fig. 10) contradicted our expectations and fell out of the hierarchy (Fig. 12A). How could the reduced expression of either *ato* or *sens* proneural genes in the *mid-RNAi* background recover bristles rather than enhance bristle loss? We were equally confounded by the apparent lack of a cell autonomous functional role for *mid* within PNs even though we detected high levels of *Mid* expression in all PNs within the 3°L eye disc (Fig. 4).

It was becoming evident that *mid* was regulating one or more complex developmental events specific to bristle generation and guided by genetic signaling hierarchies independent of the *Notch–Delta* hierarchy specifying SOP cell fates. The most viable hypothesis reconciling all of these data is that *mid* functions in a cell non-autonomous manner to regulate specific gene expression critical for the simultaneous selection and patterning of nascent precursor cells of pre-SOP cells either within or anterior of the MF during the 3°L stage of development. We have tentatively named these hypothetical precursor cells grandmother pre-SOP cells or GPS-cells as an acronym suggesting they mark a position to be tracked during subsequent stages of eye development; the GPS cells precede ganglion mother cells (GMCs) that divide to generate daughter cells of the bristle complex. We have no absolute proof of their existence, but they provide a rational explanation for the paradoxical results we obtained, challenging the idea that *mid* is only essential during early pupal stages of eye development to specify SOP cell fates.

By making the assumption that *Mid* expression within R1–R8 PN clusters is required for the expression and/or secretion of a posterior to anterior Hh morphogenic gradient regulating *dpp* and *ato* expression in both the pre-proneural and proneural zones (Bao, 2010), we can tentatively assign *mid* the cell non-autonomous function of selecting GPS-cells (Fig. 12C). We now further define GPS-cells as selected precursor cells endowed with neural competence, but prevented from transitioning into pre-SOP cells until exposed to proper morphogenic signal(s) within the proneural zone. Until key experiments are completed, we present the idea that pre-SOP cells are “tag alongs” meaning they are located proximal to the same group of progenitor cells maturing successively within and posterior of the MF that give rise to the R8 founder cell. They may either proliferate during the second wave of

mitotic division along with other progenitor cells posterior of the MF to increase their numbers (Bao, 2010) or they may not proliferate by entering stasis. Within the schematic illustrated in Fig. 12C, we place pre-SOP cells close to Ato-expressing IGs and subsequently, proximal to the R8 equivalence group and then to the R8 founder cell in columns posterior of the furrow. Frankfort et al. (2004) detected the reiterative alignment of SOP cells positioned next to R8/R7 pairs within ommatidial columns posterior of the MF.

If *mid* is required for establishing the posterior to anterior Hh gradient, we predict that the Dpp concentration required to select GPS-cells in the pre-proneural zone is either disrupted or decreased in *mid-RNAi* eye imaginal discs. As a result, the expression of *emc* and *ato* is reduced and this may hamper GPS-cell selection. In the proneural zone of *mid-RNAi* eye discs, Dpp and Dl expression is inhibited. In partial agreement, we detected reduced Dl expression within *mid-RNAi* eye discs and *H15/mid* null clones generated across the MF (Fig. 8D–F and G–I). Reduced Dpp and Dl signaling is predicted to result in greater *Emc* expression and the sequestration of Ato (Fig. 12C). In a parallel pathway, decreased levels of Dpp may also result in less *ato* expression (Fig. 12C). Although these combined outcomes should reduce the overall level of *ato* expression within the MF, reductions of Ato within the furrow were difficult to detect in *mid-RNAi* discs (Fig. 9M). Pending additional studies, we can only speculate that a compensatory signal recovered *ato* expression within the MF under *mid-RNAi* conditions.

Upon examining the Ato expression pattern within *UAS-mid-RNAi/+;ato¹/GMR-Gal4* eye discs, however, we consistently detected an apparent expansion of diffuse Ato expression across the MF occurring at the expense of Ato-expressing cell types within the proneural zone including IGs, R8 equivalence cells and pre-R8s (Fig. 9N). Ato expansion within *UAS-mid-RNAi/+;ato¹/GMR-Gal4* eye discs was divided by a characteristic band of unlabeled cells (Fig. 9N). In contrast, decreased Ato expression in the proneural zone of *UAS-mid-RNAi/+;ato¹/GMR-Gal4* discs had no effect on the selection of the pre-R8 PN or specification of PNs posterior of the MF (data not shown). This result agrees with previous data confirming that *Mid* is not essential for the specification of PNs (Supplementary Table S2).

3.4. *mid* and *emc* function within a genetic hierarchy known to regulate *ato* expression within the MF and hypothesized to select pre-SOP cells

Based upon the hypothesis that *mid* regulates *ato* expression as an upstream activator of Hh- and Dpp-activated signaling pathways within cells located in the pre-proneuronal and proneuronal zones of the 3°L eye imaginal disc, we can explain why a major recovery of bristles in *UAS-mid-RNAi/+;emc¹/GMR-Gal4* eyes may have occurred (Fig. 7E and H–J). Under these genetic conditions, the level of Dpp required to increase *emc* expression within the pre-proneural zone was compromised. As a result, *emc* expression was reduced allowing Ato to target proneural gene expression. Removing an extra 50% dosage of *emc* in *UAS-mid-RNAi/+;emc¹/GMR-Gal4* eye discs further contributed to a large reduction of *emc* expression concomitant with increased levels of activated Ato. As a consequence, GPS-cells were selected in the pre-proneural zone contributing to a significant recovery of bristles in *UAS-mid-RNAi/+;emc¹/GMR-Gal4* adult compound eyes. The selection process appears to

depend on Ato activity and as such, may require a specific, threshold level of Ato to commence.

3.5. Making sense out of senseless

Using similar logic linking Mid activity to the induction of Hh and Dpp signaling pathways, we understand why placing a heterozygous mutation of *sens* in the *mid-RNAi* background may have recovered bristles even though the recovery was less significant than that observed in *UAS-mid-RNAi/+;emc¹/GMR-Gal4* eye discs (Fig. 9E and H–J). Under *mid-RNAi* conditions we detected decreased Ac (Fig. 6A–C) and Sens expression (Fig. 6D–F) within SOP cells of pupal eye discs confirming that Mid is required for inducing proneural gene expression in SOP cells. However, we were unable to detect a change in Sens expression within mitotic clones null for *H15/mid* in either 3°L or early-staged pupal discs (data not shown). Upon reviewing the data, we realized that the randomly generated *H15/mid* mitotic clones were not large enough to span the MF and clip both anterior and posterior regions of the furrow to adequately test the model of *mid*-regulated pre-SOP selection, a model we recently developed after completing the study. At present, we are generating larger *H15/mid* null clones of this nature (spanning within and on either side of the furrow) within pupal eye discs using the Minute technique to determine whether Sens expression is reduced downstream of Hh within SOP cells (Blair, 2003). Basically, we must assay the cell non-autonomous role of *mid* to regulate *sens* expression posterior of the MF. Sens is absolutely required for the acquisition of the SOP cell fate (Frankfort et al., 2004).

3.6 Addressing a caveat of the pre-SOP selection model

The caveat of all the assumptions made thus far is that if *mid* is required to select GPS-cells which become specified into SOP cells, why did reduced levels of *ato* and *sens* within *UAS-mid-RNAi/+;ato¹/GMR-Gal4* and *UAS-mid-RNAi/+;sens^{E2}/GMR-Gal4* eye discs partially recover bristles measure by an ~16% (Fig. 9) and ~18% (Fig. 10) increase of IOBs, respectively? The recovery of bristles, although significant, was not substantial (Figs. 9 and 10). While reduced levels of *ato* and *sens* in the *mid-RNAi* background recovered pre-SOP cells during the 3°L stage, a subpopulation of these cells may not have transitioned successfully into GMCs after exiting stasis. We were likely detecting final bristle counts within each condition from two opposing effects: a gain of pre-SOP cells during the 3°L stage followed by the misspecification of SOP cells during the pupal stage. This represents a “mixed effect.” In comparison, the nearly complete recovery of bristles in *UAS-mid-RNAi/+;emc¹/GMR-Gal4* eyes measured as an ~25% increase of IOBs indicates that the selection of GMC-cells and specification of pre-SOP cells were both recovered for a net gain of bristles (Fig. 7). Finally, to add greater complexity to the interpretation of all these data, regulatory events were linked to apoptotic signaling pathways. Thus, the careful dissection of several major signaling pathways is required to understand *mid* function as a cell-fate determinant, pattern generator and pro-survival factor during specific stages of eye development.

3.7. Coming full circle: a mid GOF eye phenotype resembles a Notch LOF phenotype

Overexpressing *mid* in the eye disc using the *GMR-Gal4* driver (*UAS-mid/+;GMR-Gal4/+*) resulted in higher levels of Mid expression within R1–R8 PN clusters of 3°L eye discs without any perturbations in their arrangements or numbers (data not shown). Again, based upon the *Notch–Delta* lateral inhibition mechanism in which *mid* functions to specify SOP cell fates (Fig. 12A), SOP cells are predicted to transition to higher numbers of GMCs at the expense of epithelial cells within *UAS-mid/+;GMR-Gal4/+ UAS-mid/+;GMR-Gal4/+* discs due to a secondary *Notch* LOF phenotype. The GMC lineage would then generate shaft cells at the expense of socket cells from the PIIa daughter cell (Figs. 3C' and 12A). Sensory neurons would be generated at the expense of sheath cells from PIIb cells resulting in a smoothed eye phenotype (Fig. 3C'). The phenotype of the *UAS-mid* adult eye resembles a reported *Notch* LOF mutant eye tissue with a smoothed surface, small shaft cells and a loss of bristles (Fig. 3C') (Ye and Fortini, 1999). However, further immunolabeling and morphological studies with high cellular resolution are required to examine whether these misspecification events occur under *mid* GOF conditions since we are observing external eye features. In addition, the differentiation of PNs, the development of accessory cells or the adhesion properties of specific cells within the eye disc may also change under *mid* GOF conditions. Future studies will also test the model of GPS-cell selection within *mid* GOF tissues.

4. Conclusions

We have discovered that Mid functions within the Notch–Delta signaling pathway to specify neuronal SOP cell-fates within the pupal eye imaginal disc. This finding will update an established model of SOP cell fate specification in developing eye tissues. We also gathered indirect evidence suggesting that Mid regulates one or more morphogen gradients within the 3°L eye disc to hypothetically select and position GPS-cells in a stereotypic pattern across the ommatidial hexagonal array before they acquire neuronal specification as GMCs giving rise to bristle cell lineages. As a result, we have the unique opportunity to understand how bristles achieve their exact positions in the adult eye with fairly straightforward experimental approaches. We also determined that during the SOP cell fate specification period, when excess cells are removed by Notch–regulated apoptosis to pattern the retina, Mid inhibits apoptotic pathways. While the T-box protein family is large and functionally diverse across metazoan species, no other T-box protein has been shown to regulate apoptosis although many T-box family members are implicated in the etiology of specific cancers (Takashima and Suzuki, 2013).

Since it is evident that Mid plays multiple and overlapping functional roles within signaling pathways that guide retinal development, the goal of future studies will be to decipher the basic underpinnings of Mid function as a cell-fate determinant, pattern generator and newly identified anti-apoptotic factor within developing *Drosophila* eye tissues using a combination of highly focused genetic, molecular biological, bioinformatics and biochemical approaches to address its context-dependent activity. These foundational studies will also contribute to the knowledge base of conserved Tbx20 function in vertebrate

eye tissues including humans and may also unravel complex mechanisms regulating cellular homeostasis.

4.1. Experimental procedures

4.1.1. Fly stocks—*Drosophila melanogaster* strains were maintained at 25 °C on standard cornmeal-yeast-agar media. *Oregon-R* flies were used as wild-type (WT) and the following lines were obtained from the Bloomington Stock Center (Bloomington, Indiana):

1. Df(3L)ED4196
2. Df(3L)H99,kni^{rl}-¹P^P/TM3,Sb¹
3. mwh¹juv¹pnr^{D1}/TM2
4. w¹¹¹⁸;st¹pnr^{vx4}e¹/TM3,P{ActGFP}JMR2,Ser¹
5. w*;emc¹P{neoFRT}80B/TM6, Tb¹
6. H¹/In(3R)C e¹
7. w*;ato¹/TM6B,Tb¹
8. h¹
9. E(spl)m8-HLH¹
10. sens^{E2}red¹e¹/TM6B,Tb⁺
11. da¹pr¹cn¹/SM5
12. Su(H)¹/In(2L)Cy,ln(2R)Cy,Cy¹pr¹
13. y¹ac¹v¹
14. P{UAS-N.U}
15. y¹w*;P{Gal4}54C
16. P{UAS-p35.H}BH3,w;+/+/+/+

We used the *UAS-Gal4* system (Brand and Perrimon, 1993) and the eye-specific driver *GMR-Gal4* balanced on chromosomes II and III (a gift from Tanya Wolff; Hay et al., 1994) to express the following transgenes in WT and specific mutant backgrounds: *UAS-mid* and *UAS-mid-RNAi* (provided by Rolf Bodmer; Qian et al., 2005). The *scabrous-gal4;prospero-gal4* transgenic line was used to express *UAS-mid-RNAi* in SOP cells and their daughter cells (provided by James Skeath; Nakao and Campos-Ortega, 1996; Shiga et al., 1996). Transgenic lines used for the mosaic clonal analyses in Supplemental Figs. S3 and S4 are of the following genotypes: *y w hsFLP;H15^{vx4}mid^{la5}-FRT40A/y⁺ ry⁺ 25F FRT40A* and *y w hsFLP; H15X4mid^{la5} FRT40A/ w⁺GFP FRT 40A* (provided by William Brooks; Svendsen et al., 2009). All crosses were performed at 25 °C. We followed published procedures for generating mitotic clones within 3°L (Xu and Rubin, 1993; Svendsen et al., 2009). We isolated progeny of the genotype *UAS-mid-RNAi/+;GMR-Gal4/ato¹* by crossing *UAS-mid-RNAi/UAS-mid-RNAi;GMR-Gal4/GMR-Gal4* to *+/+;ato¹/TM6B-Tb* (*Tubby*; dominant marker) flies and simply selecting *UAS-mid-RNAi/+;GMR-Gal4/ato¹* non-*Tubby* 3°L

progeny which are longer and thinner than larvae exhibiting the short, fat Tubby phenotype (*UAS-mid-RNAi/+;GMR-Gal4/TM6B-Tb*).

4.2. Preliminary genetic modifier screen

We screened a fraction of isogenized *DrosDel* deficiency lines obtained from the Bloomington Stock Center by crossing each line to *UAS-nmr2-RNAi/CyO;GMR-Gal4/TM3 (mid-RNAi)* flies exhibiting a sensitized genetic mutation for *mid* characterized by an approximate 50% decrease of bristle complexes. Bristles were counted from 1-day old female progeny generated from the cross that were maintained at 25 °C within a humidified biological incubator under a 12 h light:dark cycle. Groups of five flies of the genotype *UAS-mid-RNAi/+;GMRGal4/Df(3)* were transfixed to a slide with clear nail polish lacquer and submerged in water to prevent light scattering. The complete eye field was viewed under a high-power Leica M165C stereomicroscope. A series of images were collected along 10–15 focal planes and digitally recorded with a Leica DFC camera. These images were flattened to create a final montage using Image Pro Plus software to correct for eye curvature and to digitally tag bristles for accurate quantification (Media Cybernetics Inc., Bethesda, MD). Implementing these methods, we identified several deficiency lines that modified the *mid* mutant phenotype (unpublished data).

4.3. Overlapping chromosomal deficiency mapping

Flies heterozygous for the *DrosDel* line *Df(3L)ED207* (61C9–62A6) significantly suppressed the *mid* mutant phenotype while flies heterozygous for *Df(3L)ED4196* (61C7-62A2) did not modify the *mid* mutant phenotype. A deficiency line developed by the Bloomington Stock Center with a heterozygous chromosomal deletion removing interval 61C8-61D2 (*Df(3L)BSC632*) significantly suppressed the *mid* mutant phenotype narrowing the region harboring *mid* suppressors to within this interval. The results also indicate that intervals 61C7 and 61D3-62A2 contain one or more second site suppressors of the putative *mid*-suppressing gene uncovered from 61C8-61D2. Upon surveying 60 gene candidates deleted within the 61C8-61D2 cytological region, we proceeded to a biased genetic modifier assay to determine whether *emc* was a *mid*-interacting gene candidate. The *emc* gene was reported to regulate SOP cell and IOB complex generation within the developing eye (flybase.org). Previous research also showed that *emc* functioned within the Notch–Delta pathway of SOP cell fate specification (Ellis et al., 1990). Further studies are underway to complete overlapping deficiency analyses of *Df(3L)ED207* to identify other potential gene candidates that modify the *mid* mutant phenotype.

4.4. Immunolabeling studies

Eye imaginal discs were dissected from developmentally staged third-instar larvae in cold phosphate buffered saline (PBS) and fixed in 3.7% paraformaldehyde in 0.1 M MOPS buffer (pH 7) for 15 min at 25 °C (Panin et al., 1997) followed by two washes of PBS containing 0.1% Triton-X 100 (PTX) and three washes of PTX supplemented with 1% bovine serum albumin (PBT). Discs were incubated in PBT containing 1% goat serum for at least one hour at 25 °C and then incubated with primary antibodies for 4 h at 25 °C or overnight at 4 °C. Pupal eye imaginal discs were developmentally staged from either timed collections of

embryos laid for a 15–30 min period from a population cage or by collecting wandering third-instar larvae and staging pupae for unique features characterizing the P1 (0–1 h APF), P2 (1–3 h APF) and P3 stages (3–6 h APF) (Bainbridge and Bownes, 1981). The P1 stage was dissected in cold PBS before fixation. The P2- and P3-staged pupal eye discs were dissected in PEMF buffer containing 0.1 M PIPES (pH 7.0), 1 mM MgSO₄, 2 mM EGTA and 3.7% paraformaldehyde (per communication with Graeme Mardon; Carroll and Whyte, 1989). P1-P3 discs were then fixed in PEMF buffer with 4% paraformaldehyde for 30 min on ice under continuous shaking followed by three 10 min washes with PAXD buffer (PBS supplemented with 1% bovine serum albumin, 0.3% Triton X-100 and 3% sodium deoxycholate) (Walther and Pichaud, 2006). Fixed discs were incubated with primary antibodies for 4 h at 25 °C or overnight at 4 °C.

We used the following primary antibodies at the indicated dilutions for this study: mouse anti-Achaetae (1:2; from Teresa Orenic, The University of Illinois, Chicago IL) (Skeath and Carroll, 1991), guinea pig anti-Atonal (1:1000; from Dave Marendia, Drexel University, Philadelphia, PA) (Melicharek et al., 2008), mouse anti-Boss (1:1000; from Larry Zipursky, HHMI, The University of California, Los Angeles, CA and Ross Cagan, Mount Sinai School of Medicine, New York (Cagan et al., 1992), guinea pig anti-extramacrochaetae (1:8000; from Yuh Nung Jan, HHMI, University of California, San Francisco, CA) (Younger-Shepherd et al., 1992), guinea pig anti-Numb (1:1000; from James Skeath, Washington University School of Medicine, St. Louis MO) (Skeath and Doe, 1998), guinea pig anti-Senseless (1:800; from Hugo Bellon, HHMI, Baylor School of Medicine, Houston, TX) (Nolo et al., 2000), guinea pig anti-H15 (1:2000), rabbit anti-Mid (1:500) (Leal et al., 2009), goat anti-Actin (1:500; Santa Cruz Biotechnology), rabbit anti-Caspase and rabbit anti-Rab5 (1:500; Abcam).

The following monoclonal antibodies were obtained from the Developmental Studies Hybridoma Bank developed under the auspices of the National Institute of Child Health and Development at The University of Iowa: anti-Armadillo (1:10) (Riggleman et al., 1990); anti-Boss (1:20) (Cagan et al., 1992), anti-DE-Cadherin (1:10) (Oda et al., 1994), anti-Cut (1:10) (Blochlinger et al., 1990), anti-Elav (1:10) (Robinow and White, 1991), anti-Delta extracellular domain (1:10; Qi et al., 1999), anti-Lozenge (1:10) (Lebestky et al., 2000), anti-Notch, extracellular domain, EGF repeats #12–20 (1:10; Diederich et al., 1994), anti-Notch, intracellular domain (1:1000; Fehon et al., 1991), anti-Repo (1:10; Jones et al., 1995) and anti-Scabrous (1:10; Lee et al., 1996). We used Alexafluor 488, 594 and 633 secondary antibodies with appropriate species specificity for immunofluorescent labeling (Molecular Probes). Eye discs were labeled with 4',6 diamino-2 phenylindole (DAPI) (1 µg/ml in PTX) for 15 min and washed 3 times with PTX for detection of nuclei. Fluorescently labeled tissues were mounted in 50% 1,4-Diazabicyclo[2.2.2]octane (DABCO) in glycerol. Paraformaldehyde, Triton X-100 and glycerol were purchased from Fisher Scientific. All other chemicals and goat pre-immune serum were obtained from Sigma–Aldrich (St. Louis, MO).

4.5. Confocal scanning microscopy

Confocal images were captured by a Zeiss LSM510 META confocal microscope and analyzed using the accompanying Zeiss LSM Image Browser software (version 5).

4.6. Scanning electron microscopy

Compound eyes of 1-day old adult flies were platinum sputter coated to a thickness of 20 nm. High-resolution images were acquired on an FEI (FEI Company, Hollisboro, OR) Quanta 200 scanning electron microscope with an accelerating voltage of 20 kV (The Department of High Performance Materials and Polymers, USM).

4.7. Statistical analyses

The mean, standard deviation and standard errors of the mean were calculated using Microsoft Excel software. The IOB counts for each genotype were statistically analyzed using Shapiro-Wilk's test for measuring the normal distribution of each data set (JMP10 software, SAS Institute Inc.). We also estimated the equal variance between groups using the Bartlett's test. Data sets that met the assumptions of a normal distribution and equal variance were then analyzed using the two-sample, two-tailed pooled Student's *t*-test. Data sets exhibiting unequal variance were analyzed using the two-sample, two-tailed unpaired Student's *t*-test. Data sets with an unequal distribution were analyzed by the Wilcoxon rank-sum test. All the probability values were calculated setting the level of significance (α) to 0.05. The data represented in the bar graph of Supplementary Fig. S2 SP were statistically analyzed using the 'ANOVA Single Factor' function to compare the means between groups. The probability value was calculated setting the level of significance (α) to 0.05 and the degree of freedom (*df*) to 1.

4.8. Software programs

Confocal scanning images were assembled using Adobe Photoshop CS6 software (Adobe Systems, Inc.). We used GraphPad Software, Inc. (La Jolla, CA) to represent data in bar charts. SEM images were cropped and scaled using Image Pro Plus software.

Supplementary Material

Refer to Web version on PubMed Central for supplementary material.

Acknowledgments

We appreciate Baobin Kang's assistance in confocal microscopy training (MS INBRE Facility's Manager, USM). We wish to acknowledge Petra Visic, Wisam Buti and Kelly Odom for assisting with overlapping chromosomal deficiency analyses. We thank Graeme Mardon for recommendations on the dissection and fixation of pupal eye imaginal discs. We are grateful to the following colleagues for providing antibodies: Hugo Bellon for anti-Senseless antibody, David Marenda for anti-Atonal antibody, Teresa Orenic for anti-Ac monoclonal antibody, Ross Cagan and Larry Zipursky for anti-Boss antibody and Jan Yun for anti-Emc antibody. We also wish to thank Rolf Bodmer, Li Qian, William Brooks, James Skeath, Tanya Wolff and the Bloomington Stock Center (Bloomington, IN) for fly stocks. We gratefully acknowledge Philip C. Kolin, University Distinguished Professor in the College of Arts and Letters (USM), for expert editing of the manuscript. Confocal microscopy was supported by the Mississippi INBRE funded by grants from the National Center for Research Resources (5P20RR-016476-11) and the National Institute of General Medical Sciences from the National Institutes of Health (8 P20 GM103476-11) to Glenmore Shearer (USM). R.T. was supported by a REU from the Alliance for Graduate Education in Mississippi awarded by the National Science Foundation (NSF) (ID HRD-0450362). This research study was supported by a NSF Research

Initiation Grant to S.M.L. (ID 920625). SML dedicates this publication to Dr. Jung San Huang who taught her the “gongfu of science.”

REFERENCES

- Adam JC, Montell DJ. A role of extra macrochaetae downstream of Notch in follicle cell differentiation. *Development*. 2004; 131:5971–5980. [PubMed: 15539491]
- Affolter M, Nellen D, Nussbaumer U, Basler K. Multiple requirements for the receptor serine/threonine kinase thick veins reveal novel functions of TBF beta homologs during *Drosophila* embryogenesis. *Development*. 1994; 120:3105–3117. [PubMed: 7720555]
- Artavanis-Tsakonas S, Matsuno K, Fortini ME. Notch signaling. *Science*. 1995; 268:225–232. [PubMed: 7716513]
- Bainbridge SP, Bownes M. Staging the metamorphosis of *Drosophila melanogaster*. *J. Embryol. Exp. Morph.* 1981; 65:57–80. [PubMed: 6801175]
- Baker NE, Zitron AE. *Drosophila* eye development: Notch and Delta amplify a neurogenic pattern conferred on the morphogenetic furrow by scabrous. *Mech. Dev.* 1995; 49:173–189. [PubMed: 7734391]
- Bao, S. Two themes on the assembly of the *Drosophila* eye.. In: Cagan, RL.; Reh, TA., editors. *Invertebrate and Vertebrate Eye Development*. Academic Press, Elsevier Inc.; San Diego CA: 2010. p. 85-117.
- Baonza A, Garcia-Bellido A. Dual role of extramacrochaetae in cell proliferation and cell differentiation during wing morphogenesis in *Drosophila*. *Mech. Dev.* 1999; 80:133–146. [PubMed: 10072780]
- Baonza A, deCelis JF, Garcia-Bellido A. Relationships between extramacrochaetae and Notch signaling in *Drosophila* wing development. *Development*. 2000; 127:2383–2393. [PubMed: 10804180]
- Blochlinger KR, Bodmer R, Jan LY, Jan YN. Patterns of expression of Cut, a protein required for external sensory organ development in wild-type and cut mutant *Drosophila* embryos. *Nature*. 1990; 333:629–635. [PubMed: 2897632]
- Bhattacharya A, Baker NE. A network of broadly expressed HLH genes regulates tissue-specific cell fates. *Cell*. 2011; 147:881–892. [PubMed: 22078884]
- Blair S. Genetic mosaic techniques for studying *Drosophila* development. *Development*. 2003; 130:5065–5072. [PubMed: 12975340]
- Bossuyt W, De Geest N, Aerts S, Leenaerts I, Marynen P, Hassan BA. The atonal proneural transcription factor links differentiation and tumor formation in *Drosophila*. *PLoS Biol.* 2009; 7(2):e40. [PubMed: 19243220]
- Brand AH, Perrimon N. Targeted gene expression as a means of altering cell fates and generating dominant phenotypes. *Development*. 1993; 118:401–415. [PubMed: 8223268]
- Brown NL, Sattler CA, Markey DR, Carroll SB. Hairy gene function in the *Drosophila* eye: normal expression is dispensable but ectopic expression alters cell fates. *Development*. 1991; 113:1245–1256. [PubMed: 1811940]
- Buescher M, Svendsen PC, Tio M, Miskolczi-McCallum C, Tear G, Brook WJ, Chia W. *Drosophila* T box proteins break the symmetry of hedgehog-dependent activation of wingless. *Curr. Bio.* 2004; 14:1694–1702. [PubMed: 15458640]
- Buescher M, Tio M, Tear G, Overton PM, Brook WJ, Chia W. Functions of the segment polarity genes *midline* and *H15* in *Drosophila melanogaster* neurogenesis. *Dev. Biol.* 2006; 292:418–429. [PubMed: 16499900]
- Cadigan KM, Nusse R. Wingless signaling in the *Drosophila* eye and embryonic epidermis. *Development*. 1996; 122:2801–2812. [PubMed: 8787754]
- Cadigan KM, Jou AD, Nusse R. Wingless blocks bristle formation and morphogenetic furrow progression in the eye through repression of Daughterless. *Development*. 2002; 129:3393–3402. [PubMed: 12091309]
- Cagan RL, Ready DF. Notch is required for successive cell decisions in the developing *Drosophila* retina. *Genes Dev.* 1989a; 3:1099–1112. [PubMed: 2792755]

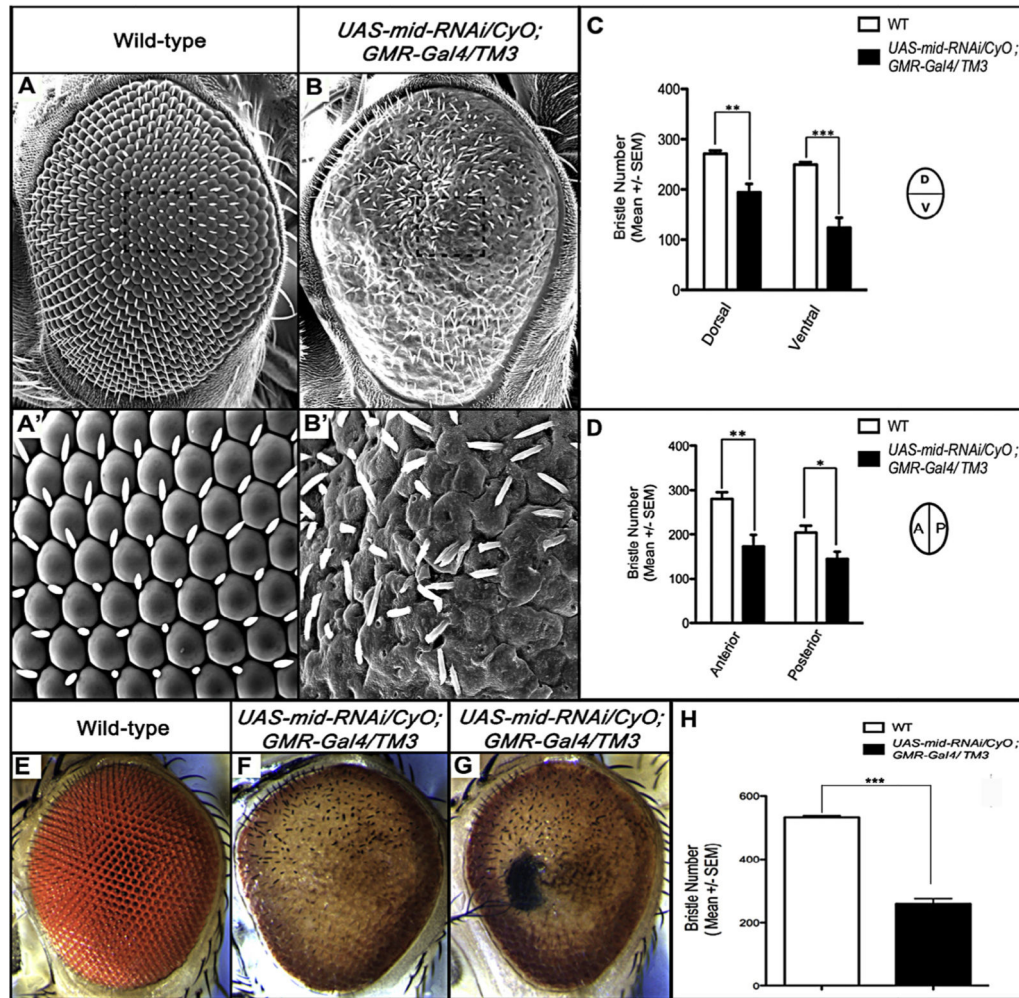
- Cagan RL, Ready DF. The emergence of order in the *Drosophila* pupal retina. *Dev. Biol.* 1989b; 136:346–362. [PubMed: 2511048]
- Cagan RL, Kramer H, Hart AC, Zipursky SL. The bride of sevenless and sevenless interaction: internalization of a transmembrane ligand. *Cell.* 1992; 69:393–399. [PubMed: 1316239]
- Carroll SB, Whyte JS. The role of the hairy gene during *Drosophila* morphogenesis: stripes in imaginal discs. *Development.* 1989; 3:905–916.
- Chandrasekaran V, Beckendorf SK. Senseless is necessary for survival of embryonic salivary glands in *Drosophila*. *Development.* 2003; 130:4719–4728. [PubMed: 12925597]
- Chen P, Nordstrom W, Gish B, Abrams JM. Grim, a novel cell death gene in *Drosophila*. *Genes Dev.* 1996; 10:1773–1782. [PubMed: 8698237]
- Copeland JM, Bosdet I, Freeman JD, Guo M, Gorski SM, Hay BA. Echinus, required for interommatidial cell sorting and cell death in the *Drosophila* pupal retina, encodes a protein with homology to ubiquitin-specific proteases. *BMC Dev. Bio.* 2007; 7:82. [PubMed: 17612403]
- Cubas P, de Celis JF, Campuzano S, Modolell J. Proneural clusters of *achaete-scute* expression and the generation of sensory organs in the *Drosophila* wing imaginal disc. *Genes Dev.* 1991; 5:996–1008. [PubMed: 2044965]
- Cutforth T, Gaul U. The genetics of visual system development in *Drosophila*: specification, connectivity and asymmetry. *Curr. Opin. Neurobiol.* 1997; 7:48–54. [PubMed: 9039792]
- DeStrooper B, Annaert W, Cupers P, Saftig P, Craessaerts K, Mumm JS, Schroeter EH, Schrijvers V, Wolfe MS, Ray WJ, Goate A, Kopan R. A presenilin-1-dependent gamma-secretase-like protease mediates release of Notch intracellular domain. *Nature.* 1999; 398:518–522. [PubMed: 10206645]
- Dichtel-Danjoy ML, Ma D, Dourlen P, Chatelain G, Napoletano F, Robin M, Corbet M, Levet C, Hafsi H, Hainaut P, Ryoo HD, Bourdon JC, Mollereau B. *Drosophila* p53 isoforms differentially regulate apoptosis and apoptosis-induced proliferation. *Cell Death Differ.* 2013; 20:108–116. [PubMed: 22898807]
- Diederich RJ, Matsuno K, Hing H, Artavanis-Tsakonas S. Cytosolic interaction between deltex and Notch ankyrin repeats implicates deltex in the Notch signaling pathway. *Development.* 1994; 120:473–481. [PubMed: 8162848]
- Dokucu ME, Zipursky SL, Cagan RL. Atonal, Rough and the resolution of proneural clusters in the developing *Drosophila* retina. *Development.* 1996; 122:4139–4147. [PubMed: 9012533]
- Doroquez DB, Rebay I. Signal integration during development: mechanisms of EGFR and Notch pathway function and cross-talk. *Crit. Rev. Biochem. Mol. Biol.* 2006; 41:339–385. [PubMed: 17092823]
- Ellis HM, Spann DR, Posakony JW. *Extramacrochaetae*, a negative regulator of sensory organ development in *Drosophila* defines a new class of helix-loop-helix proteins. *Cell.* 1990; 61:27–38. [PubMed: 1690604]
- Ellis MC, O'Neill EM, Rubin GM. Expression of *Drosophila* glass protein and evidence for negative regulation of its activity in non-neuronal cells by another DNA-binding protein. *Development.* 1993; 119:855–865. [PubMed: 8187644]
- Fehon RG, Kooh PJ, Rebay I, Artavanis-Tsakonas S. Complex cellular and subcellular regulation of Notch expression during embryonic and imaginal development of *Drosophila*: Implications for Notch function. *J. Cell Biol.* 1991; 113:657–669. [PubMed: 2016340]
- Frankfort BJ, Mardon G. R8 development in the *Drosophila* eye: a paradigm for neural selection and differentiation. *Development.* 2002; 129:1295–1306. [PubMed: 11880339]
- Frankfort BJ, Pepple KL, Mamlouk M, Rose MF, Mardon G. Senseless is required for pupal retinal development in *Drosophila*. *Genesis.* 2004; 38:182–194. [PubMed: 15083519]
- Freeman M. Reiterative use of the EGF receptor triggers differentiation of all cell types in the *Drosophila* eye. *Cell.* 1996; 87:651–660. [PubMed: 8929534]
- Freeman M. Cell determination strategies in the *Drosophila* eye. *Development.* 1997; 124:261–270. [PubMed: 9053303]
- Garrell J, Modolell J. The *Drosophila extra-macrochaetae* locus, an antagonist of proneural genes that, like these genes, encodes a helix-loop-helix protein. *Cell.* 1990; 61:39–48. [PubMed: 1690605]

- Go MJ, Eastman DS, Artavanis-Tsakonas S. Cell proliferation control by Notch signaling in *Drosophila* development. *Development*. 1998; 125:2031–2040. [PubMed: 9570768]
- Grether ME, Abrams JM, Agapite J, White K, Stellar H. The *head involution defective* gene of *Drosophila melanogaster* functions in programmed cell death. *Genes Dev*. 1995; 9:1694–1708. [PubMed: 7622034]
- Guo M, Jan LY, Jan YN. Control of daughter cell fates during asymmetric division: interaction of Numb and Notch. *Neuron*. 1996; 17:27–41. [PubMed: 8755476]
- Hagedorn EJ, Bayraktar JL, Kandachar VR, Bai T, Englert DM, Chang HC. *Drosophila melanogaster* auxin regulates the internalization of Delta to control activity of the Notch signaling pathway. *J. Cell Bio*. 2006; 173:443–452. [PubMed: 16682530]
- Hay BA, Wolff T, Rubin GM. Expression of Baculovirus P35 prevents cell death in *Drosophila*. *Development*. 1994; 120:2121–2129. [PubMed: 7925015]
- Heberlein U, Wolff T, Rubin GM. The TGF beta homolog *dpp* and the segment polarity gene *hedgehog* are required for propagation of a morphogenetic wave in the *Drosophila* retina. *Cell*. 1993; 75:913–926. [PubMed: 8252627]
- Heitzler P, Haenlin M, Romain P, Calleja M, Simpson P. A genetic analysis of *pannier*, a gene necessary for viability of dorsal tissues and bristle positioning in *Drosophila*. *Genetics*. 1996; 143:1271–1286. [PubMed: 8807299]
- Jafar-Nejad H, Acar M, Nolo R, Lacin H, Pan H, Parkhurst SM, Bellon HJ. *Senseless* acts as a binary switch during sensory organ precursor selection. *Genes Dev*. 2003; 17:2966–2978. [PubMed: 14665671]
- Jahangiri L, Nelson AC, Wardle FC. A cis-regulatory module upstream of *deltaC* regulated by *Ntla* and *Tbx16* drives expression in the tailbud, presomitic mesoderm and somites. *Dev. Biol*. 2012; 371:110–120. [PubMed: 22877946]
- Jarman AP, Grell EH, Acherman L, Jan LY, Jan YN. *Atonal* is the proneural gene for *Drosophila* photoreceptors. *Nature*. 1994; 369:398–400. [PubMed: 8196767]
- Jarman AP, Sun Y, Jan LY, Jan YN. Role of the proneural gene, *atonal*, in formation of *Drosophila* chordotonal organs and photoreceptors. *Development*. 1995; 121:2019–2030. [PubMed: 7635049]
- Jones BW, Fetter RD, Tear G, Goodman CS. Glial cells missing: a genetic switch that controls glial versus neuronal fate. *Cell*. 1995; 82:1013–1023. [PubMed: 7553843]
- Koto A, Kuranaga E, Miura M. Apoptosis ensures spacing pattern formation of *Drosophila* sensory organs. *Curr. Biol*. 2011; 21:2780287.
- Kraus F, Haenig B, Kispert A. Cloning and expression analysis of the mouse T-box gene *Tbx20*. *Mech. Dev*. 2001; 100:87–91. [PubMed: 11118890]
- Kumar JP. Building an ommatidium one cell at a time. *Dev. Dyn*. 2012; 241:136–149. [PubMed: 22174084]
- LaCount DJ, Hanson SF, Schneider CL, Friesen PD. Caspase inhibitor P35 and inhibitor of apoptosis Op-IAP block in vivo proteolytic activation of an effector caspase at different steps. *J. Biol. Chem*. 2000; 275:15657–15664. [PubMed: 10747956]
- Lai EC, Orgogozo V. A hidden program in *Drosophila* peripheral neurogenesis revealed: fundamental principles underlying sensory organ diversity. *Dev. Biol*. 2004; 269:1–17. [PubMed: 15081353]
- Leal SM, Qian L, Lacin H, Bodmer R, Skeath JB. *Neuromancer1* and *Neuromancer2* Regulate Cell Fate Specification in the Developing Embryonic CNS of *Drosophila melanogaster*. *Dev. Biol*. 2009; 325:138–150. [PubMed: 19013145]
- Lebestky T, Chang T, Hartenstein V, Banerjee U. Specification of *Drosophila* hematopoietic lineage by conserved transcription factors. *Science*. 2000; 288:146–149. [PubMed: 10753120]
- Lee E, Hu X, Yu S, Baker NE. The secreted glycoprotein *scabrous* regulates proneural development in the *Drosophila* eye. *Mol. Cell. Biol*. 1996; 16:1179–1188. [PubMed: 8622662]
- Li W-Z, Li S-L, Zheng HY, Zhang S-P, Xue L. A broad expression profile of the *GMR-Gal4* driver in *Drosophila melanogaster*. *Genet. Mol. Res*. 2012; 11:1997–2002. [PubMed: 22911584]
- Ligoxygakis P, Yu SY, Delidakis C, Baker NE. A subset of notch functions during *Drosophila* eye development require *Su(H)* and the *E(spl)* gene complex. *Development*. 1998; 125:2893–2900. [PubMed: 9655811]

- Lovicu FJ, McAvoy JW, de longh RU. Understanding the role of growth factors in embryonic development: insights from the lens. *Philos. Trans. R. Soc. Lond. B.* 2011; 366:1204–1218. [PubMed: 21402581]
- Lyman DF, Yedvobnick B. *Drosophila* Notch receptor activity suppresses Hairless function during adult external sensory organ development. *Genetics.* 1995; 141:1491–1505. [PubMed: 8601489]
- Meins M, Henderson DJ, Bhattacharya SS, Sowden JC. Characterization of the human TBX20 gene, a new member of the T-box gene family closely related to the *Drosophila* H15 gene. *Genomics.* 2000; 67:317–332. [PubMed: 10936053]
- Melicharek D, Shah A, DiStefano G, Gangemi AJ, Orapallo A, Vrailas-Mortimer AD, Marena DA. Identification of novel regulators of *atonal* expression in the developing *Drosophila* retina. *Genetics.* 2008; 180:2095–2110. [PubMed: 18832354]
- Mesquita D, Dekanty A, Milan M. A dp53-dependent mechanism involved in coordinating tissue growth in *Drosophila*. *PLoS Biol.* 2010; 8:e10000566.
- Miller DT, Cagan RL. Local induction of patterning and programmed cell death in the developing *Drosophila* retina. *Development.* 1988; 125:2327–2335. [PubMed: 9584131]
- Mok LP, Qin T, Bardot B, LeComte M, Homayouni A, Ahimou F, Wesley C. Delta activity independent of its activity as a ligand of Notch. *BMC Dev. Biol.* 2005; 5:6. [PubMed: 15760463]
- Mollereau B, Domingos PM. Photoreceptor differentiation in *Drosophila*: from immature neurons to functional receptors. *Dev. Dyn.* 2005; 232:585–592. [PubMed: 15704118]
- Moses K, Ellis MC, Rubin GM. The *glass* gene encoded a zinc-finger protein required by *Drosophila* photoreceptor cells. *Nature.* 1989; 340:531–536. [PubMed: 2770860]
- Muller D, Kugler SJ, Preiss A, Maier D, Nagel AC. Genetic modifier screens on *Hairless* gain-of-function phenotypes reveal genes involved in cell differentiation, cell growth and apoptosis in *Drosophila melanogaster*. *Genetics.* 2005; 171:1137–1152. [PubMed: 16118195]
- Muskavitch MA. Delta-notch signaling and *Drosophila* cell fate choice. *Dev. Biol.* 1994; 166:415–430. [PubMed: 7813766]
- Nagaraj R, Banerjee U. Combinatorial signaling in the specification of primary pigment cells in the *Drosophila* eye. *Development.* 2007; 134:825–831. [PubMed: 17251265]
- Nakao K, Campos-Ortega JA. Persistent expression of genes of the *enhancer of split* complex suppresses neural development in *Drosophila*. *Neuron.* 1996; 16:272–286.
- Nolo R, Abbott LA, Bellon HJ. Senseless, a Zn finger transcription factor, is necessary and sufficient for sensory organ development in *Drosophila*. *Cell.* 2000; 102:349–362. [PubMed: 10975525]
- Oda H, Uemura T, Harada Y, Iwai Y, Takeichi M. A *Drosophila* homolog of Cadherin associated with Armadillo and essential for embryonic cell–cell adhesion. *Dev. Biol.* 1994; 165:716–726. [PubMed: 7958432]
- Ohsako S, Hyer J, Panganiban G, Oliver I, Caudy M. Hairy function as a DNA-binding helix-loop-helix repressor of *Drosophila* sensory organ formation. *Genes Dev.* 1994; 8:2743–2755. [PubMed: 7958930]
- Panin VM, Papayannopoulos V, Wilson R, Irvine KD. Fringe modulates Notch-ligand interactions. *Nature.* 1997; 387:908–912. [PubMed: 9202123]
- Parks AL, Turner FR, Muskavitch MAT. Relationships between complex Delta expression and the specification of retinal cell fates during *Drosophila* eye development. *Mech. Dev.* 1995; 50:201–216. [PubMed: 7619731]
- Parody TR, Muskavitch MA. The pleiotropic function of Delta during postembryonic development of *Drosophila melanogaster*. *Genetics.* 1993; 135:527–539. [PubMed: 8244012]
- Pepple KL, Atkins M, Venken K, Wellnitz K, Harding M, Franfort B, Mardon G. Two-step selection of a single R8 photoreceptor: a bistable loop between *senseless* and *rough* locks in R8 fate. *Development.* 2008; 135:4071–4079. [PubMed: 19004852]
- Pickup AT, Lamka ML, Sun Q, Yip MLR, Lipshitz HD. Control of photoreceptor cell morphology, planar polarity and epithelial integrity during *Drosophila* eye development. *Development.* 2002; 129:2247–2258. [PubMed: 11959832]
- Qi H, Rand MD, Wu X, Sestan N, Wang W, Rakic P, Xu T, Artavanis-Tsakonas S. Processing of the notch ligand delta by the metalloprotease Kuzbanian. *Science.* 1999; 283:91–94. [PubMed: 9872749]

- Qian L, Liu J, Bodmer R. Neuromancer TBX20-related genes (*H15/midline*) promote cell fate specification and morphogenesis of the *Drosophila* heart. *Dev. Biol.* 2005; 279:509–524. [PubMed: 15733676]
- Ramain P, Heitzler P, Haenlin M, Simpson P. *Pannier*, a negative regulator of achaete and scute in *Drosophila*, encodes a zinc finger protein with homology to the vertebrate transcription factor GATA-1. *Development.* 1993; 119:1277–1291. [PubMed: 7916679]
- Ready DF, Hanson TE, Benzer S. Development of the *Drosophila* retina, a neurocrystalline lattice. *Dev. Biol.* 1976; 53:217–240. [PubMed: 825400]
- Rebeiz M, Miller SW, Posakony JW. Notch regulates numb: integration of conditional and autonomous cell fate specification. *Development.* 2011; 138:215–225. [PubMed: 21148185]
- Robinow S, White K. Characterization and spatial distribution of the ELAV protein during *Drosophila melanogaster* development. *J. Neurobiol.* 1991; 22:443–461. [PubMed: 1716300]
- Rutkowski R, Hofmann K, Gartner A. Phylogeny and function of the invertebrate p53 superfamily. *Cold Spring Harb. Perspect. Biol.* 2010; 2:a001131. Epub. [PubMed: 20595397]
- Schroeter EH, Kisslinger JA, Kopan R. Notch-1 signalling requires ligand-induced proteolytic release of intracellular domain. *Nature.* 1998; 393:382–386. [PubMed: 9620803]
- Schweisguth F. Regulation of notch signaling activity. *Curr. Bio.* 2004; 14:R129–R138. [PubMed: 14986688]
- Shiga Y, Tanaka-Matakatsu M, Hayashi S. A nuclear GFP/ beta-galactosidase fusion protein as a marker of morphogenesis in living *Drosophila*. *Dev. Growth Differ.* 1996; 38:99–106.
- Silver RJ, Rebay I. Signaling circuitries in development: insights from the retinal determination network. *Development.* 2005; 132:3–13. [PubMed: 15590745]
- Skeath JB, Carroll SB. Regulation of achaete–scute gene expression and sensory organ pattern formation in the *Drosophila* wing. *Genes Dev.* 1991; 5:984–995. [PubMed: 2044964]
- Skeath JB, Doe CQ. Sanpodo and Notch act in opposition to Numb to distinguish sibling fates in the *Drosophila* CNS. *Development.* 1998; 125:1857–1865. [PubMed: 9550718]
- Smith JE 3rd, Cronmiller C. The *Drosophila daughterless* gene autoregulates and is controlled by both negative and positive gene regulation. *Development.* 2001; 128:4705–4714. [PubMed: 11731451]
- Svensden PC, Formaz-Preston A, Leal SM, Brook WJ. The Tbx20 homologs *midline* and *H15* specify ventral fate in the *Drosophila melanogaster* leg. *Development.* 2009; 136:2689–2693. [PubMed: 19605497]
- Takashima Y, Suzuki A. Regulation of organogenesis and stem cell properties by T-box transcription factors. *Cell Mol. Life Sci.* 2013 Epub.
- Tomlinson A, Ready DF. Cell fate in the *Drosophila* ommatidium. *Dev. Biol.* 1987; 123:264–275. [PubMed: 17985474]
- Tripathi BJ, Tripathi RC, Livingston AM, Borisuth NS. The role of growth factors in the embryogenesis and differentiation of the eye. *Am. J. Anat.* 1991; 192:442–471. [PubMed: 1781453]
- Tsachaki M, Sprecher SG. Genetic and developmental mechanisms underlying the formation of the *Drosophila* compound eye. *Dev. Dyn.* 2012; 241:40–56. [PubMed: 21932322]
- van Doren M, Ellis HM, Posakony JW. The *Drosophila* extramacrochaetae protein antagonizes sequence-specific DNA binding by daughterless/achaete–scute protein complexes. *Development.* 1991; 113:245–255. [PubMed: 1764999]
- Vuong L, Conley SM, Al-Ubaidi MR. Expression and role of p53 in the retina. *Invest. Ophthalmol. Vis. Sci.* 2012; 53:1362–1371. [PubMed: 22427613]
- Waddington CH, Perry MM. The ultrastructure of the developing eye of *Drosophila*. *Proc. R. Soc. Biol. Sci.* 1960; 153:155–178.
- Walther RF, Pichaud F. Immunofluorescent staining and imaging of the pupal and adult *Drosophila* visual system. *Nat. Protoc.* 2006; 1:2635–2642. [PubMed: 17406519]
- White K, Grether ME, Abrams JM, Young L, Farrell K, Steller H. Genetic control of programmed cell death in *Drosophila*. *Science.* 1994; 264:677–683. [PubMed: 8171319]
- Wigglesworth VB. The origin of the sensory neurons in an insect, *Rhodnius prolixus* (Hemiptera). *Q. J. Microsc. Sci.* 1953; 94:93–112.

- Wolff T, Ready DF. Cell death in normal and rough eye mutants of *Drosophila*. *Development*. 1991; 113:825–839. [PubMed: 1821853]
- Xu T, Rubin GM. Analysis of genetic mosaics in developing and adult *Drosophila* tissues. *Development*. 1993; 117:1223–1237. [PubMed: 8404527]
- Yamaguchi M, Hirose F, Inoue YH, Shiraki M, Hayashi Y, Nishi Y, Matsukage A. Ectopic expression of human p53 inhibits entry into S phase and induces apoptosis in the *Drosophila* eye imaginal disc. *Oncogene*. 1999; 18:6767–6775. [PubMed: 10597285]
- Yao KM, Samson ML, Reeves R, White K. Gene *elav* of *Drosophila melanogaster*: a prototype for neuronal-specific RNA binding protein gene family that is conserved in flies and humans. *J. Neurobiol.* 1993; 24:723–739. [PubMed: 8331337]
- Ye Y, Fortini ME. Apoptotic activities of wild-type and Alzheimer's disease-related mutant presenilins in *Drosophila melanogaster*. *J. Cell Biol.* 1999; 146:1351–1364. [PubMed: 10491396]
- Younger-Shepherd S, Vaessin H, Bier E, Jan LY, Jan YN. *Deadpan*, an essential pan-neural gene encoding an HLH protein, acts as a denominator in *Drosophila* sex determination. *Cell*. 1992; 70:911–922. [PubMed: 1525829]
- Yu SY, Yoo SJ, Yang L, Zapata C, Srinivasan A, Hay BA. A pathway of signals regulating effector and initiator caspases in the developing *Drosophila* eye. *Development*. 2002; 129:3269–3278. [PubMed: 12070100]

**Fig. 1.**

Reducing expression of *mid* during third-instar larval and early pupal stages results in severe eye defects. Scanning electron micrograph (SEM) images of 1-day old adult eyes depict (A) a wild-type Oregon-R (OR) compound (WT) eye with a normal ommatidial array and (B) a *mid-RNAi* eye exhibiting a severe reduction of interommatidial bristles (IOBs) and a rough eye characterized by ommatidial fusion. (A') Enlarged images of the WT pattern of ommatidia and (B') a *mid-RNAi* eye detail the extent of ommatidial fusion and irregularly shaped bristles (B'). (C and D) The bar charts represent mean IOB numbers and the error bars denote the standard errors of the mean (SEM) quantitated from 10 scanning electron micrographs of WT and *mid-RNAi* eyes. (C) Comparisons of dorsal versus ventral and (D) anterior versus posterior fields of WT (white bars) and *mid-RNAi* eyes (black bars) show a significant reduction of IOBs under *mid-RNAi* conditions across all fields. The reduction of IOBs in the ventral field of *mid-RNAi* eyes compared to WT eyes is highly significant ($p^{***} < 0.0001$). Comparisons of data are indicated by brackets linking specific data sets ($p^* < 0.01$, $p^{**} < 0.001$) (E–G) Light microscope images taken at 120 \times magnification depict (E) a WT eye exhibiting a precisely patterned ommatidial array and (F) a *mid-RNAi* eye with a loss of IOBs, disorganized ommatidia and pigmentation defects. (G) An example of a *mid-*

RNAi mutant eye exhibiting scarring due to tissue degeneration. (H) The bar chart represents mean IOB numbers \pm SEM from 10 montaged images of adult fly eyes of WT and *mid-RNAi* eyes. The reduction of IOBs in *mid-RNAi* eyes is statistically significant (***) $p < 0.0001$). Statistical analyses were performed using Shapiro-Wilk's test and the Student's *t*-test.

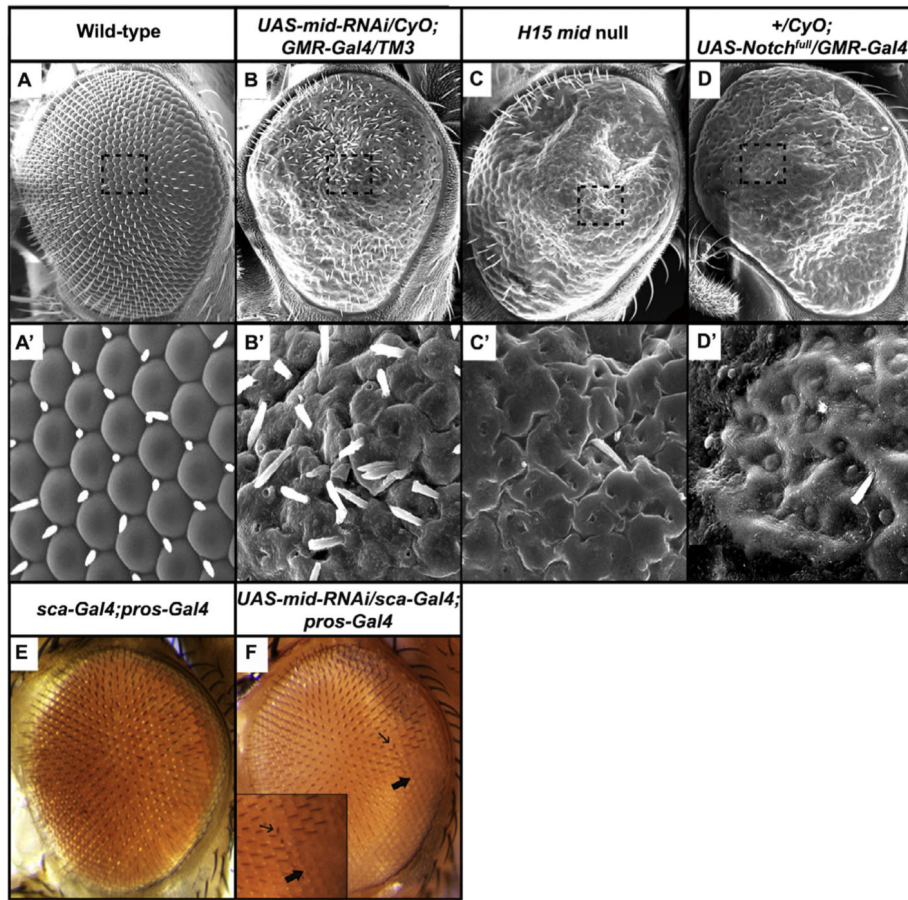


Fig. 2.

A LOF *H15/mid* null mitotic clone generated in developing eye tissues closely resembles a *Notch* gain-of-function phenotype. Scanning electron micrographs depict adult compound eyes of (A) a wild-type, (B) *mid-RNAi* and (C) a LOF *H15/mid* null mitotic clone generated during the P0–P2 pupal stages. The LOF *H15/mid* null tissue exhibits similar yet more severe mutant features observed in *mid-RNAi* eyes including the loss of IOBs and ommatidial fusion. (D) Overexpressing *Notch* using the *GMR-Gal4* line (+/CyO;*UAS-Notch*^{full}/*GMR-Gal4*) resulted in a mutant phenotype resembling tissues generated from *H15/mid* LOF clones. (E) A light microscope image at 120× of an eye from a *sca-Gal4;pros-Gal4* transgenic line showing a normal pattern of bristle loss in ommatidial columns in the posterior-most region of the eye. (F) An eye from a *UAS-mid-RNAi/sca-Gal4;pros-Gal4/TM3* fly exhibits expanded IOB loss in ommatidial columns in the posterior area (thick arrow) and IOBs that have shifted in polarity (thin arrow). The inset details these changes at a higher magnification.

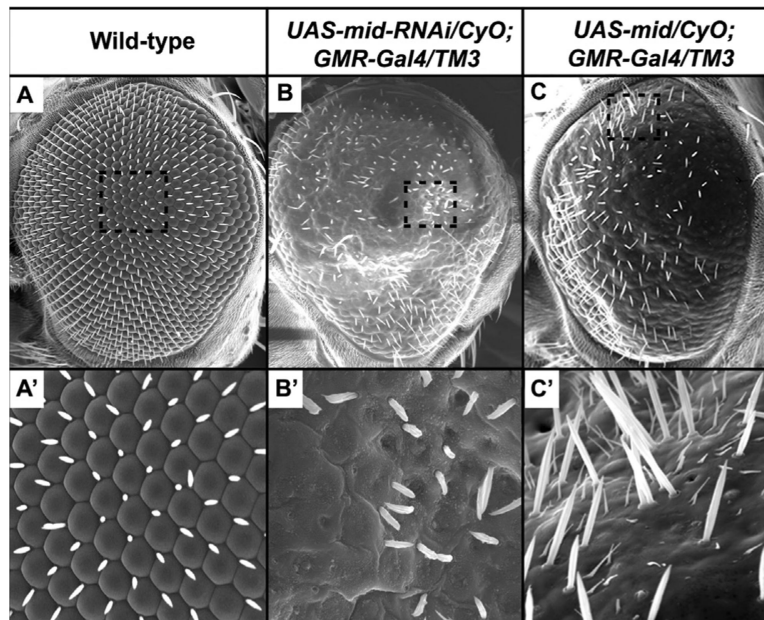


Fig. 3. A *mid* gain-of-function mutation exhibits features that are similar to a *Notch* LOF phenotype. (A–C) Scanning electron micrographs of 1-day old adult eyes depicting (A) a WT compound eye (B) a *mid-RNAi* eye and (C) a *UAS-mid/CyO;GMR-Gal4/TM3* mutant eye. Overexpressing *mid* causes bristle defects, a smoothed surface and IOB loss. (C') An enlarged image of panel C depicts an excess of socketless, small shaft cells and duplicated IOB complexes.

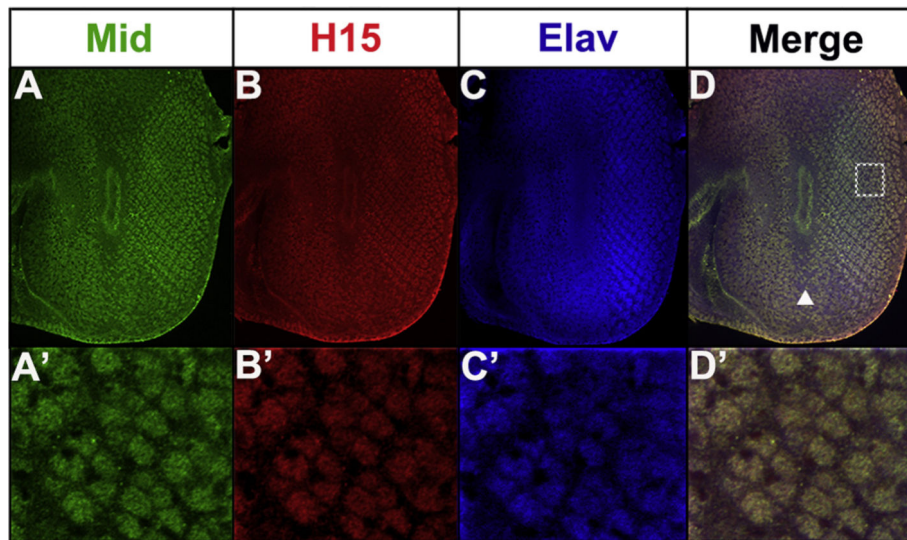


Fig. 4.

Mid, H15 and Elav are co-expressed in photoreceptor neurons of third-instar larval eye imaginal discs. Confocal images of WT third-instar larval eye discs co-immunolabeled with (A) Mid (green), (B) H15 (red) and (C) Elav (blue) antisera show that all proteins are expressed within photoreceptor neurons. (D) The merged image demonstrates that Mid, H15 and Elav are also co-expressed within photoreceptor neurons (yellow). The white arrowhead points to the MF. Posterior is right.

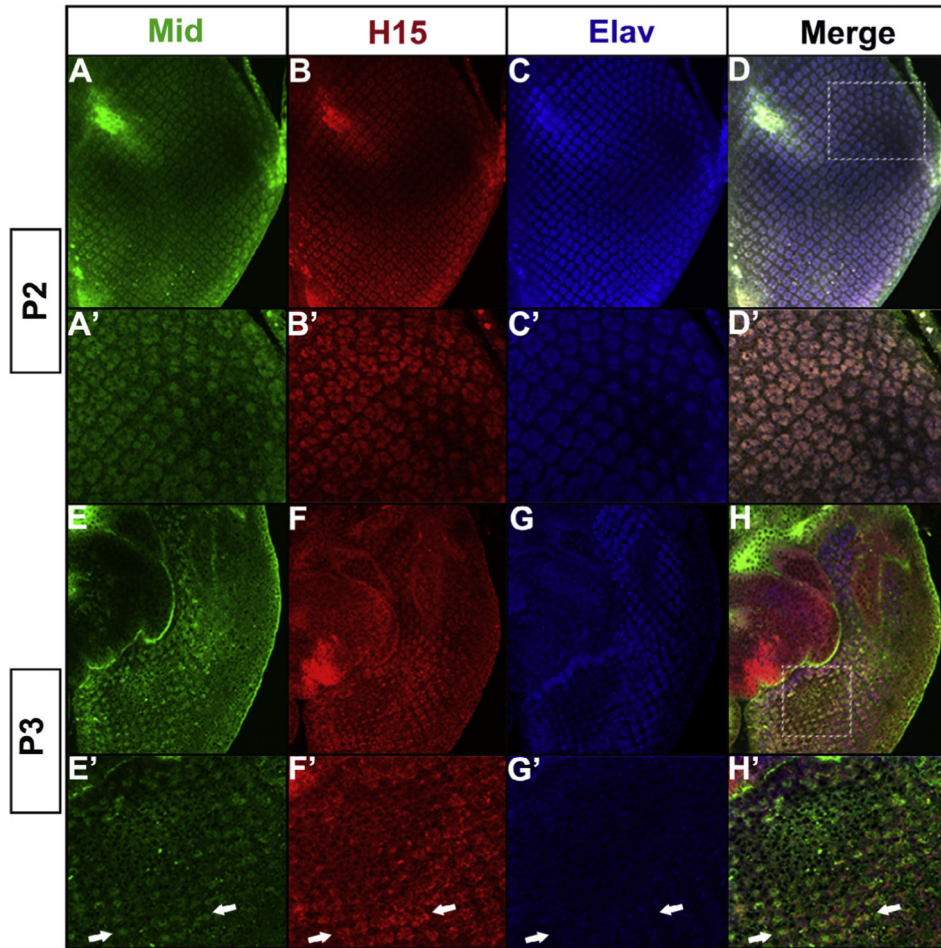


Fig. 5. Mid and H15 are co-expressed in photoreceptor neurons and sensory organ precursor cells of early-staged pupal eye imaginal discs. Confocal images of WT P2-staged pupal eye discs immunolabeled with (A) Mid (green), (B) H15 (red) and (C) Elav (blue) antisera detecting these proteins within photoreceptor neurons during the P2 stage of development. (D) The merged image shows that Mid, H15 and Elav exhibit an overlapping expression pattern within photoreceptor neurons (magenta). (A'–D') Higher magnification images of panels A–D represent the area enclosed by the dashed box in panel D. (E–H) WT P3-staged pupal eye discs are immunolabeled with (E) Mid (green), (F) H15 (red) and (G) Elav (blue) antisera. (H) The orientation of the disc as mounted reveals two unique populations of cells in one focal plane represented by the merged image. Mid, H15 and Elav expression is diminishing in photoreceptor neurons (H, merge, magenta) while a Mid- and H15-expressing population of SOP cells is also detected (arrow). (E'–H') Higher magnification images of panels E–H represent the area enclosed by the dashed boxed region shown in panel H. Posterior is to the right.

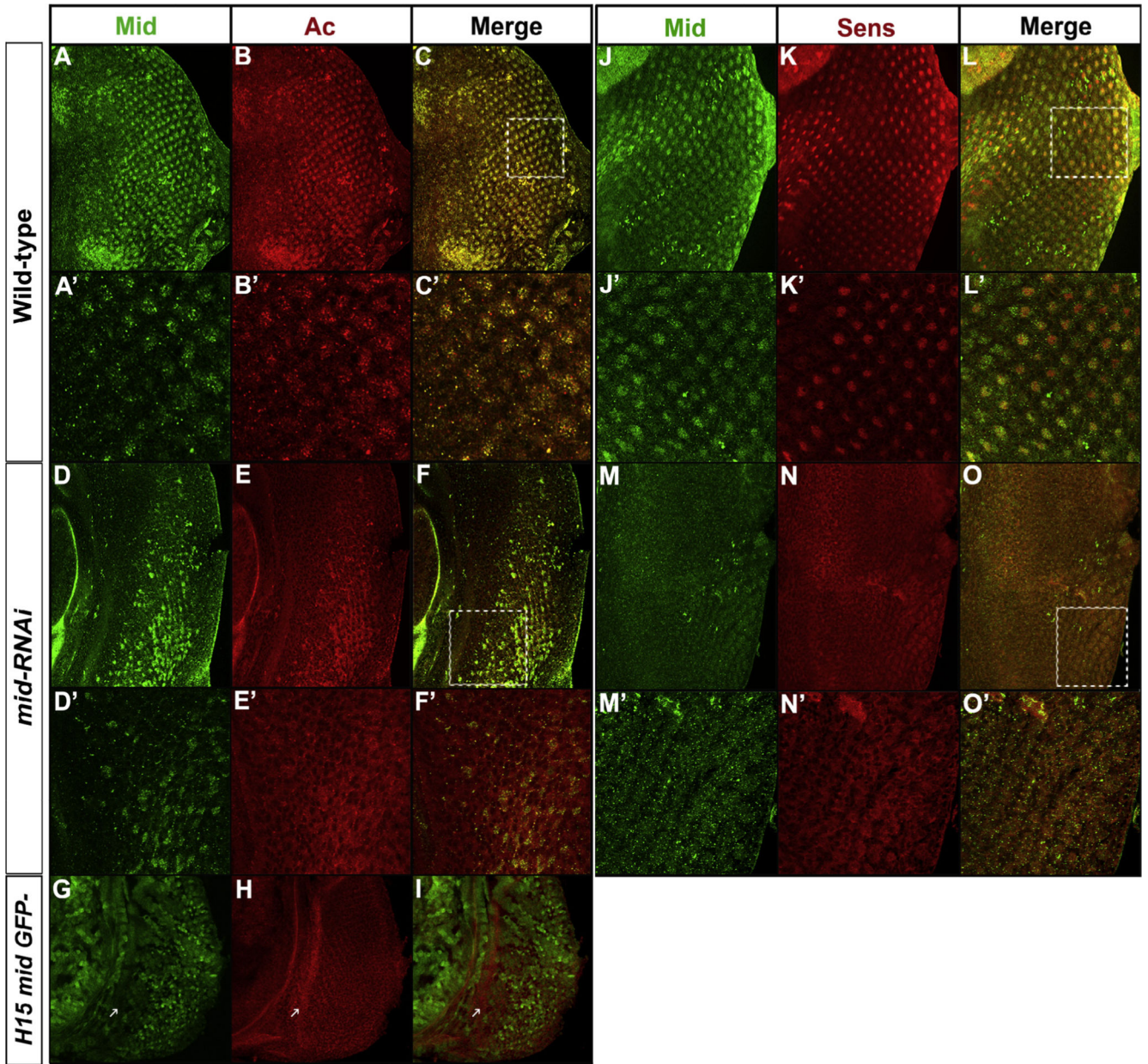


Fig. 6. *mid* regulates the expression of the proneural genes *achaetae* and *senseless*. Confocal image of a P2-staged WT pupal eye disc co-immunolabeled with (A) anti-Mid (green) and (B) anti-Ac (red) antisera shows that Mid and Ac are (C) co-expressed in SOP cells (merge). (D) A P3-staged *mid-RNAi* pupal eye disc also co-immunolabeled with (D) anti-Mid (green) and (E) anti-Ac antisera (red) depicting reduced Mid and Ac expression (merge) (F). (G–I) *H15/mid* LOF clones generated within the P3-staged eye disc are numerous. (G) *15/mid* clones (–GFP) immunolabeled with (H) anti-Ac antibody exhibit reduced expression of Ac (red). (I) A merge of panels (G) and (H) depicts extensive *H15/mid* null clones (–GFP) and *H15/mid* heterozygous mutant tissues expressing one copy of GFP (light green). (J–L) P3-staged pupal eye discs co-immunolabeled with (J) anti-Mid (green) and (K) anti-Sens (red)

antisera. (L) WT discs exhibit an overlapping Mid and Sens expression pattern marking SOPs while (M–O) *mid-RNAi* discs show decreased expression of (M) Mid and (N) Sens where (O) represents the merged image. (A'–F' and J'–O') Higher magnification images of boxed regions in panels A–F and J–O from the boxed regions (dashed). Posterior is to the right.

Author Manuscript

Author Manuscript

Author Manuscript

Author Manuscript

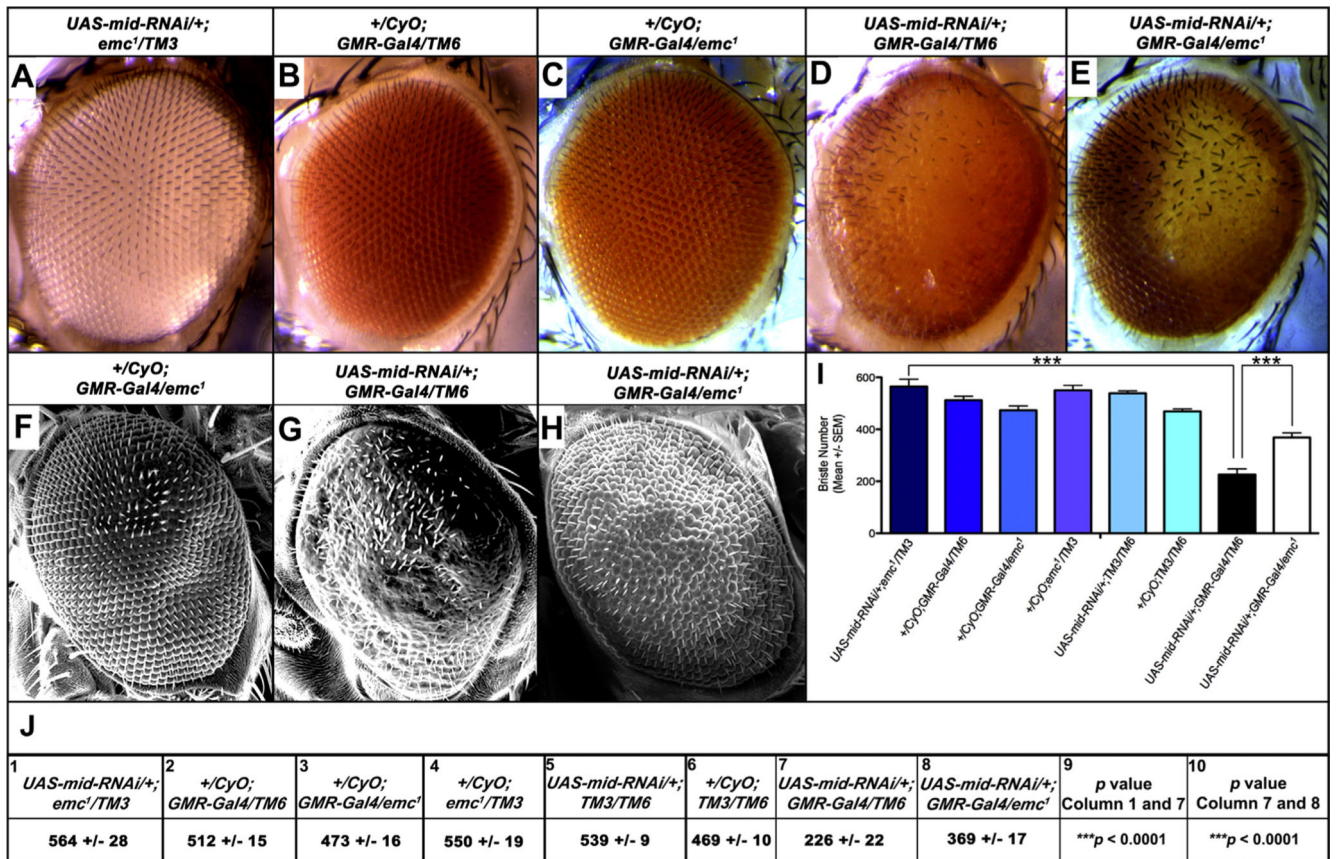


Fig. 7.

mid collaborates with *extramacrochaetae* to regulate interommatidial bristle generation. (A–E) Light microscope images at 120× magnification depict (A) *UAS-mid-RNAi/+; emc¹/TM3*, (B) *+CyO; GMR-Gal4/TM6* and (C) *+CyO; GMR-Gal4/emc¹* eyes exhibiting a well-organized ommatidial array and numbers of IOBs that are nearly equivalent to the WT OR eye phenotype. (D) A *UAS-mid-RNAi/+; GMR-Gal4/TM6* (*mid-RNAi*) eye exhibits a ~50% loss of IOBs and disorganized ommatidia. (E) Placing the heterozygous *emc¹* mutant allele in the *mid-RNAi* background to generate a *UAS-mid-RNAi/+; GMR-Gal4/emc¹* eye partially suppresses the mutant IOB phenotype by a ~25% increase in IOBs, partially recovers the integrity of the ommatidial array and restores a large area of pigmentation in the tissue. (F–H) Scanning electron micrograph images show greater details of IOBs and ommatidial arrangements. (F) The *+CyO; GMR-Gal4/emc¹* eye depicts a few duplicated bristles within the center. (G) The *mid-RNAi* eye exhibits large regions of IOB loss, ommatidial fusion and surviving IOBs are disorganized. (H) Although a few ommatidia are fused and there are size differences among them, the *UAS-mid-RNAi/+; GMR-Gal4/emc¹* eye exhibits a significant recovery of IOBs throughout the eye field. The ommatidia of the *UAS-mid-RNAi/+; GMR-Gal4/emc¹* represented in (H) were counted and nearly equal in number (701 counted) to ommatidia of WT OR eyes (750 counted). (I) The bar graph represents mean bristle numbers ± SEM quantitated for 10 eyes for each genotype shown in panels A–E as well as additional genotypes generated from the cross including *+CyO; emc¹/TM3*, *UAS-mid-RNAi/+; TM3/TM6* and *+CyO; TM3/TM6*. Comparisons of data are indicated by brackets linking

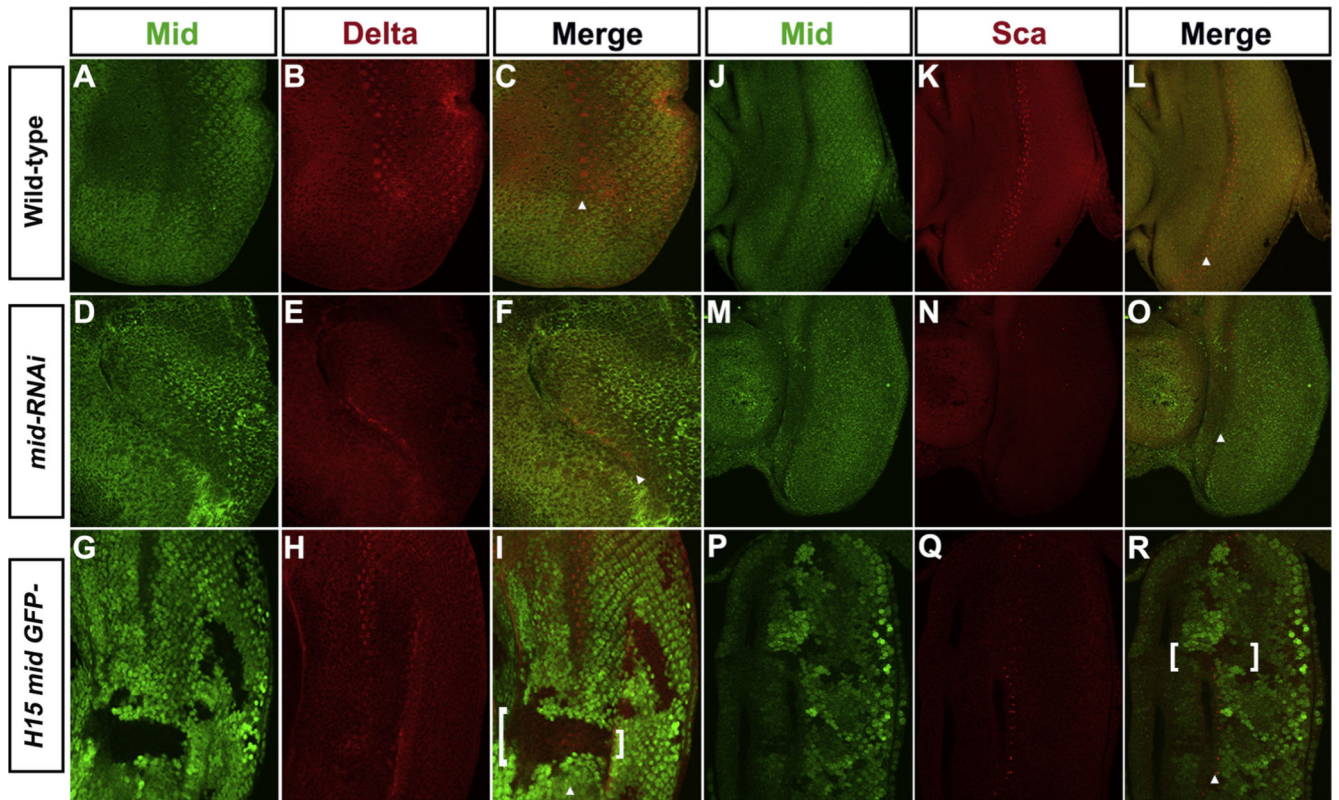
specific data sets. The full genotype of the mutant *emc¹* allele is *emc¹P{neoFRT}80B*. (J) A table with columns labeled 1–8 in the left top corners represents the mean IOB numbers \pm the SEM for each genotype represented in the bar graph. The inhibition of bristle numbers in *mid-RNAi* mutants was statistically significant comparing columns 1 versus (vs) 7 where $***p < 0.0001$. The suppression of IOB loss observed in *mid-RNAi* eyes in the absence of one functional copy of *emc* was also statistically significant comparing column 7 vs 8 where $***p < 0.0001$. Statistical analyses were performed using Shaprio-Wilk's test and the Student's *t*-test.

Author Manuscript

Author Manuscript

Author Manuscript

Author Manuscript

**Fig. 8.**

Loss of *H15/mid* results in decreased Delta and Sca expression within the MF. A confocal image of a WT 3°L eye disc co-immunolabeled with anti-Mid and anti-Delta antisera shows that (A) Delta (red) predominantly labels proneural clusters within the furrow while (B) Mid (green) is expressed predominantly within photoreceptor neurons. (C) The merged image demonstrates that Delta and Mid exhibit a mutually exclusive expression pattern. (D–F) A *mid-RNAi* disc also co-immunolabeled with anti-Mid and anti-Delta antisera depicts (D) reduced levels of Mid (green) and (E) Delta (red) expression. (F) The merged image shows that Delta is expressed within a narrow band of cells in a vaguely defined furrow. (G) A 3°L eye disc harboring several large *H15/mid* LOF clones (–GFP) is immunolabeled with (H) anti-Delta antibody. (I) In the merged image, one clone spanning the MF and extending into zones anterior and posterior of the MF (bracket) exhibits reduced expression of Delta (red) while an additional clone generated within the MF directly above but flanked with Mid-expressing tissue (green) shows a WT Delta expression pattern. (J–L) A confocal image of a WT 3°L eye disc co-immunolabeled with anti-Mid and anti-Sca antisera shows that (J) Mid (green) and (K) Sca (red) also exhibit a (L) non-overlapping expression pattern (merge). (M–O) A *mid-RNAi* disc lacks (M) Mid (green) and (N) exhibits a nearly complete loss of Sca (red) expression also detailed within the (O) merge. (P) A confocal image of *H15/mid* null clones (–GFP) generated in the 3°L eye disc. (Q) The disc is immunolabeled with anti-Sca antibody. Sca is expressed in a WT pattern within most areas of the MF and marks R8 cells posterior of the MF (Baker and Zitron, 1995). The only *H15/mid* null clone lacking Sca expression (bracket) spans the MF and extends anteriorly and posteriorly. The arrowhead shown in all panels marks the MF.

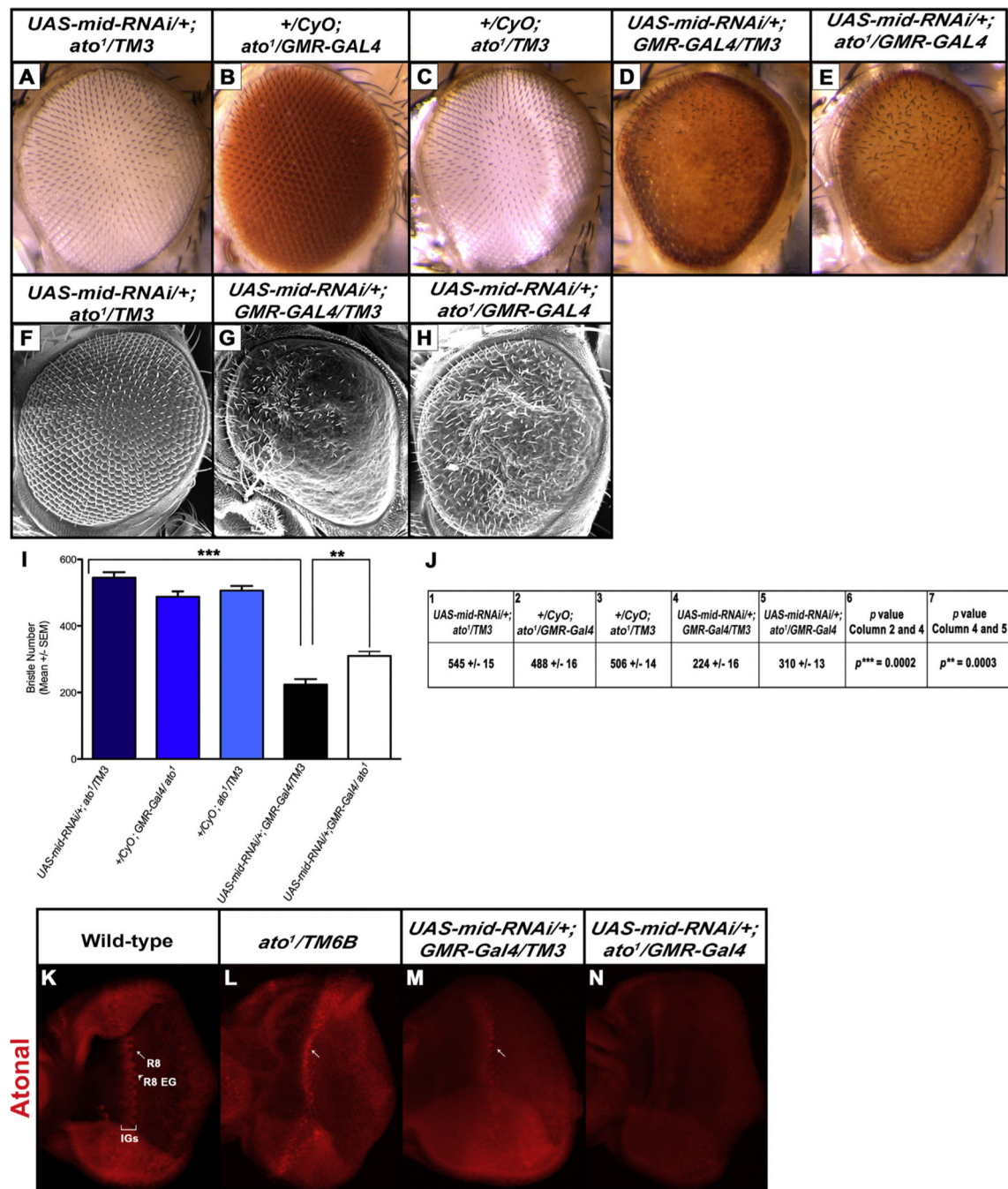


Fig. 9. *mid* collaborates with *atonal* to regulate interommatidial bristle generation. (A–E) Light microscope images at 120× magnification depict (A) *UAS-mid-RNAi/+; ato¹/TM3*, (B) *+CyO; ato¹/GMR-Gal4* and (C) *+CyO; ato¹/TM3* eyes exhibiting normal ommatidial arrays and numbers of IOBs that are nearly equivalent to those counted in the WT OR eye (Fig. 1H). (D) A *UAS-mid-RNAi/+; GMR-Gal4/TM3* (*mid-RNAi*) eye exhibits a significant loss of IOBs by ~59% and disorganized ommatidia as previously shown (Fig. 1E,H). (E) Placing the heterozygous *ato¹* mutant allele in the *mid-RNAi* genetic background to generate a *UAS-*

mid-RNAi/+;GMR-Gal4/ato¹ eye partially suppresses the mutant IOB phenotype with a ~16% gain of IOBs. The integrity of the ommatidial array is not restored and remaining IOBs are disorganized. (F–H) The scanning electron micrographs detail selected WT and mutant bristle phenotypes from panel A, D and E, respectively. (I) The bar graph represents mean bristle numbers \pm SEM quantitated from montaged light microscope images taken of 10 eyes representing each genotype shown in panels A–E. Comparisons of data are indicated by brackets linking specific data sets. (J) A table with columns labeled 1–5 in the left top corners represents the mean IOB numbers \pm the SEM for each genotype represented in the bar graph. The inhibition of bristle numbers in *mid-RNAi* mutants was statistically significant comparing column 2 vs 4 where *** $p = 0.0002$. The suppression of IOB loss observed in *mid-RNAi* eyes in the absence of one functional copy of *ato* was also statistically significant comparing column 4 vs 5 where *** $p = 0.0003$. Statistical analyses were performed using Shaprio-Wilk's test and the Student's *t*-test (K–L) Confocal images of 3°L eye discs immunolabeled with anti-Ato antibody. (K) A WT Oregon-R disc details several Ato-expressing (red) intermediate groups (IGs) (bracket) and R8-equivalence groups (R8 EGs) (arrowhead) within the MF. R8 PNs (arrow) emerge posterior of the furrow. (L) The *ato¹/TM6* and (M) *mid-RNAi* mutant discs exhibit a WT expression pattern of Ato while the (N) *UAS-mid-RNAi/+;GMR-Gal4/ato¹* mutant disc lacks the distinct labeling of Ato-expressing cell populations. Right is posterior.

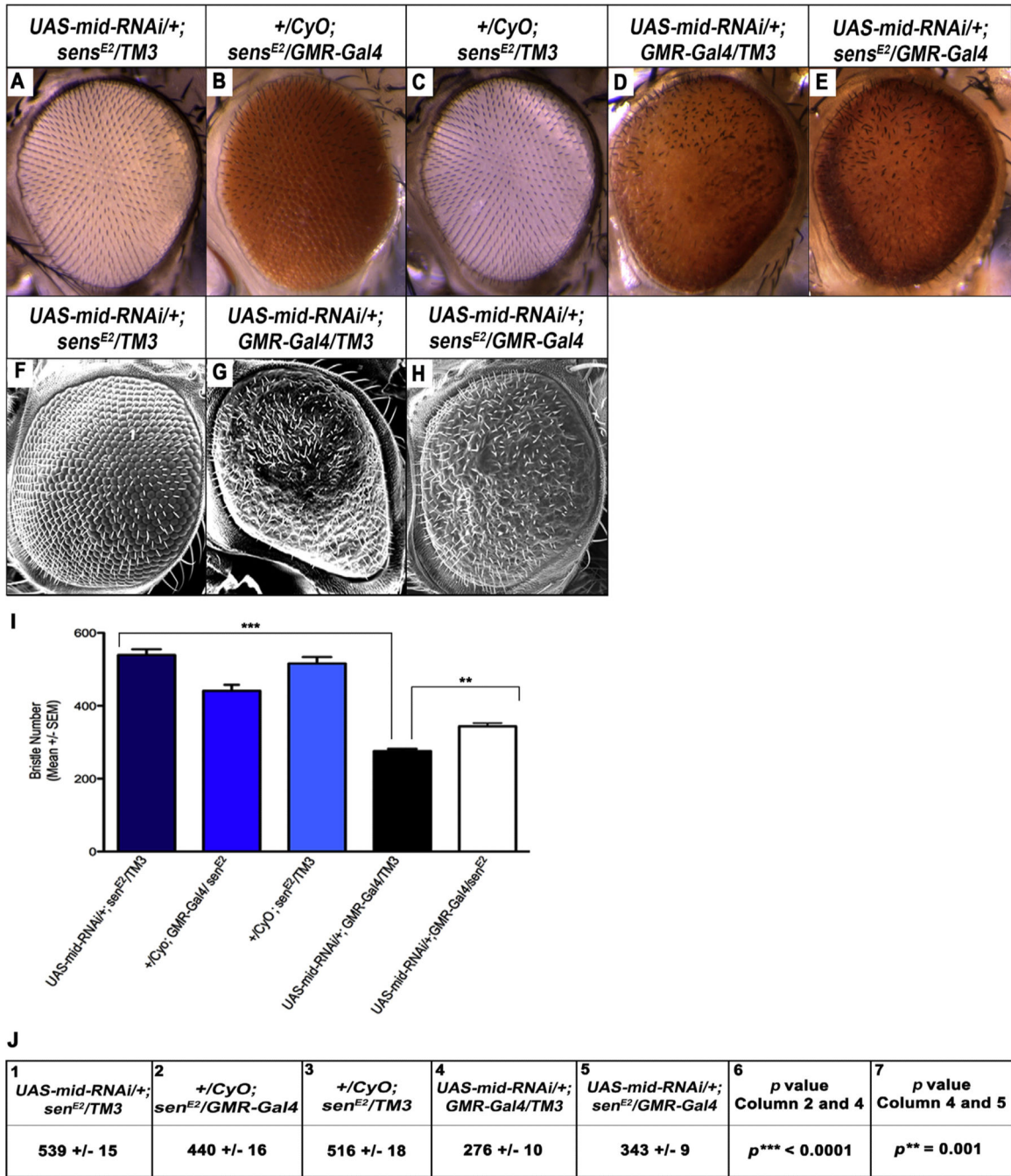


Fig. 10. *mid* collaborates with *senseless* to regulate interommatidial bristle generation. (A–E) Light microscope images at 120× magnification depict (A) *UAS-mid-RNAi/+; sens^{E2}/TM3*, (B) *+CyO; sens^{E2}/GMR-Gal4* and (C) *+CyO; sens^{E2}/TM3* mutant eyes. While eyes depicted in panels (A–C) exhibit an ommatidial array and numbers of IOBs that are nearly equivalent to the WT OR eye (Fig. 1E and H), placing a heterozygous mutant allele of (B) *sens^{E2}* in the *GMR-Gal4* background results in an ~18% loss of IOBs. (D) A *UAS-mid-RNAi/+; GMR-Gal4/TM3* (*mid-RNAi*) eye exhibits an ~49% loss of IOBs and disorganized ommatidia. (E)

Placing the heterozygous *sens*^{E2} mutant allele in the *mid-RNAi* genetic background to generate a *UAS-mid-RNAi/+;GMR-Gal4/sens*^{E2} eye partially suppresses the mutant IOB phenotype exhibited by a ~14% increase in IOBs. However, the ommatidial array and remaining IOBs are disorganized. (F–H) The scanning electron micrographs detail selected WT and mutant bristle phenotypes from panel A, D and E, respectively. (I) The bar graph represents mean bristle numbers \pm SEM quantitated for 10 montaged light microscope images eyes per each genotype shown in panels A–E. Comparisons of data are indicated by brackets linking specific data sets. The full genotype of the mutant *sens*^{E2} allele is *sens*^{E2}*red*¹*e*¹. (J) A table with columns labeled 1–5 in the left top corners represents the mean IOB numbers \pm the SEM for each genotype represented in the bar graph. The inhibition of bristle numbers in *mid-RNAi* mutants was statistically significant comparing column 2 vs 4 where ****p* < 0.0001. The suppression of IOB loss observed in *mid-RNAi* eyes in the absence of one functional copy of *sens* was also statistically significant comparing column 4 vs 5 where ***p* < 0.001. Statistical analyses were performed using Shapiro-Wilk's test and the Student's *t*-test.

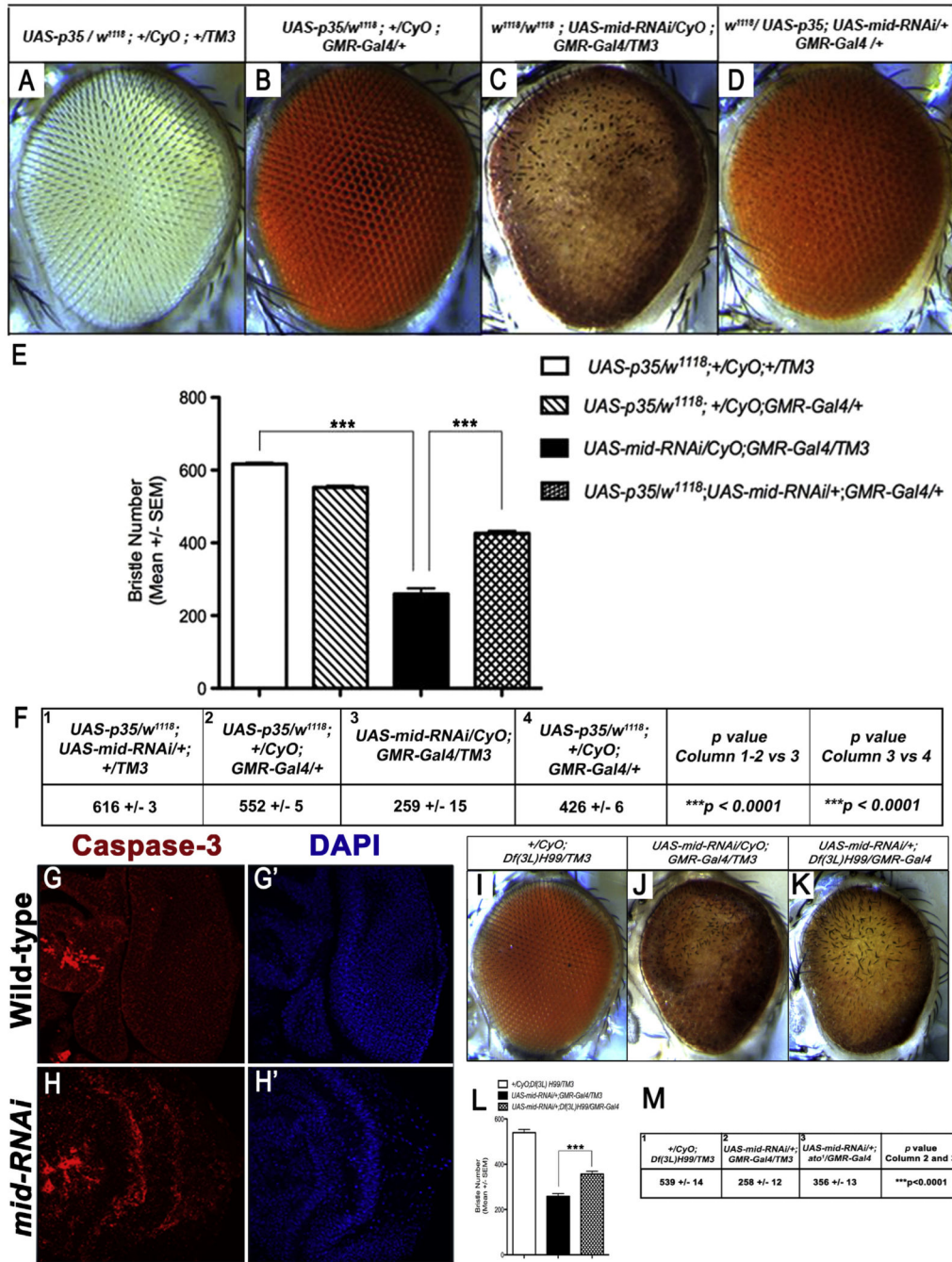


Fig. 11. Reduced expression of Mid results in apoptosis within the pupal eye imaginal disc. (A–D) Compound eyes from representative genotypes of progeny generated from crossing *UAS-p35/Y; +/+; +/+* males to *w¹¹¹⁸/w¹¹¹⁸; UAS-mid-RNAi/CyO; GMR-Gal4/TM3* (*mid-RNAi*) females. (A) *UAS-p35/w¹¹¹⁸; +/CyO; +/TM3* and (B) *UAS-p35/w¹¹¹⁸; +/CyO; GMR-Gal4/+* flies exhibit normal numbers of bristles. (C) It was not possible to obtain female *mid-RNAi* flies from the cross because the *UAS-p35* transgene is on the X-chromosome. For this reason we used parental *mid-RNAi* female flies for quantitating bristles for comparisons with other

groups. (D) $w^{1118}/UAS-p35;UAS-mid-RNAi/+;GMR-Gal4$ eyes exhibit a partial suppression of the *mid-RNAi* mutant phenotype. (E) The bar graph depicts the mean number of bristles \pm the SEM quantitated from 10 eyes from each represented genotype in panels A–D and indicates that the suppression of the *mid-RNAi* mutation by overexpressing *p35* is statistically significant ($*p < 0.0001$). Comparisons of data represented by bar charts are indicated by brackets linking specific data sets. (F) Numeric values and statistical analyses of the bar graph are presented in table format. (G) A WT P3-staged pupal eye disc co-stained with anti-Caspase-3 antibody (red) and (G') the nuclear marker DAPI (blue) exhibits a uniform array of photoreceptor neurons and SOP cells. (H) A stage-matched *mid-RNAi* pupal eye immunolabeled with anti-Caspase-3 (red) exhibits increased expression of Caspase-3 indicative of apoptosis. (H') DAPI (blue) labeling of the same *mid-RNAi* disc shows tissue degeneration. (I–K) The comparison of (I) $+/CyO;Df(3L)H99/TM3$, (J) parental $UAS-mid-RNAi/CyO;GMR-Gal4/TM3$ and (K) $UAS-mid-RNAi/+;Df(3L)H99/GMR-Gal4$ compound eyes shows that placing *mid-RNAi* in a heterozygous *Df(3L)H99* background removing one copy of the pro-apoptotic genes *grim*, *reaper* and *hid* partially recovers the *mid-RNAi* phenotype. (L) The bar graph depicts the mean number of bristles \pm the SEM quantitated from montage light microscope images of 10 eyes from each represented genotype in panels I–K and indicates that the suppression of the *mid-RNAi* mutation by overexpressing *p35* is statistically significant ($***p < 0.0001$). Comparisons of data represented by the bar graph are indicated by brackets linking specific data sets. (M) A table showing the means \pm the SEM values from the bar graph. Statistical analyses were performed using Shaprio-Wilk's test and the Student's *t*-test.

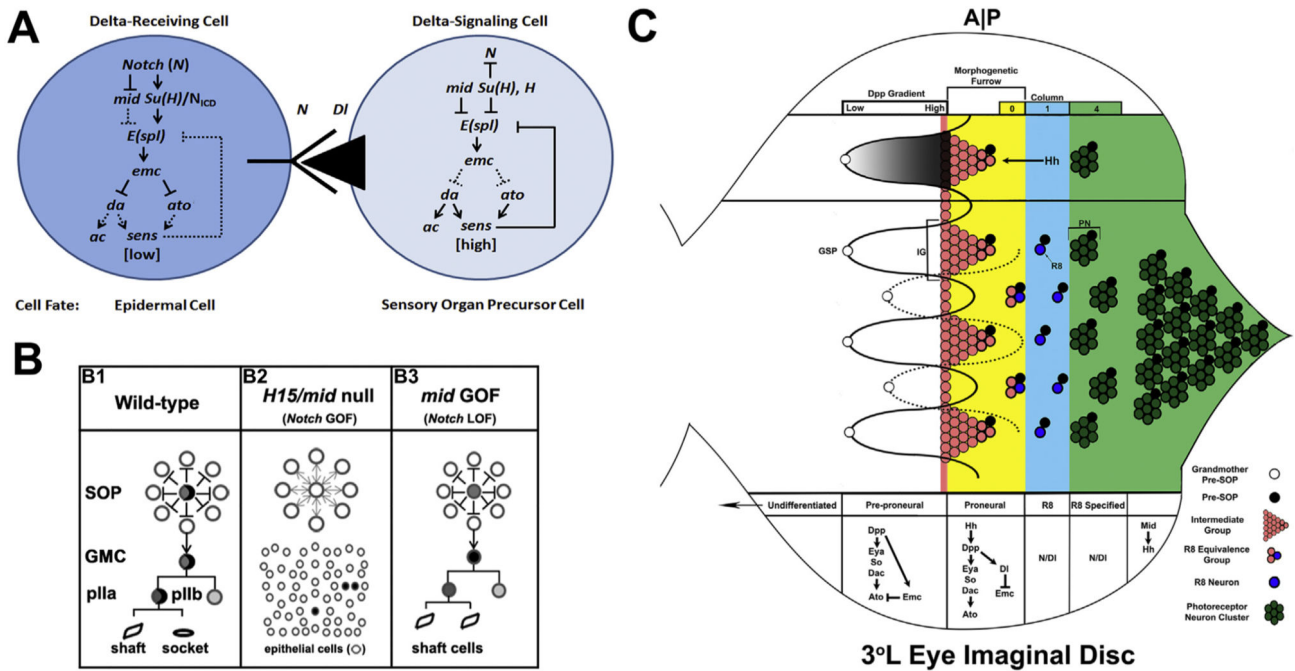


Fig. 12. Signaling pathways essential for R8 and SOP cell specification (A) Notch (N) signaling is inhibited in the SOP cell (right) by the co-repressors *Su(H)* and *H* that inhibit *E(spl)* expression. This leads to the potential reduction of *emc* expression or change in *Emc* activity. With *Emc* inactive, a subsequent increase in *da* as well as increased *ac*, *ato*, and *sens* gene expression occurs. High levels of *sens* further activate *ac* expression (Jafar-Nejad et al., 2003). Conversely, in the Delta-receiving cell (left) Notch signaling is active. *Su(H)* and the N_{ICD} activate *E(spl)* expression. *E(Spl)* then positively modulates either *emc* expression or *Emc* activity. *Emc* can now physically sequester *Da* and *Ato* resulting in reduced expression of the proneural genes *ac* and *sens*. Low levels of *sens* are predicted to inhibit *ac* expression (Jafar-Nejad et al., 2003). *mid* is placed downstream of *Notch* and upstream of both *E(Spl)* and *emc*. The dashed lines indicate a loss of *mid* that affects gene expression within the pathway. (B) A series of Notch–Delta signaling events illustrated in schematics compares WT and *mid* mutant conditions in the generation of SOP cells and SOP daughter cells. (B1) Under WT conditions, lateral inhibition by Notch–Delta signaling results in the generation of a Ganglion Mother Cell (GMC) from an SOP while neighboring cells assume the default epidermal fate. The GMC divides giving rise to the *pIIa* and *pIIb* cells. The *pIIa* cell divides to generate the shaft and socket cells. The black crescent shown in the SOP cell, GMC and *pIIa* precursor cells depicts the asymmetric inheritance of the *Numb* protein. (B2) *H15/mid* LOF mutant conditions appear to result in a *Notch* GOF phenotype that results in an abnormal expansion of epithelial cells at the expense of SOP cells. (B3) *mid* overexpression results in the generation of small shaft cells within the dorsal region of the eye from an apparent *Notch* LOF phenotype. SOP cells are duplicated at the expense of default epithelial cells (black circles) (not shown) and shaft cells are duplicated at the expense of socket cells. (C) A *Dpp* morphogenic gradient is established from the posterior (high concentration) to anterior regions of the eye imaginal disc (low

concentration) (black graded shading). Only one gradient is shown but fills the spaces in a reiterative pattern outlined below. High-affinity Dpp receptor binding sites expressed by undifferentiated cells in the pre-proneural zone (white background) may initiate the selection of Grandmother Precursor-SOP cells (GPS-cells; open circles). Low affinity Dpp receptor binding sites expressed by Ato-positive cells (pink circles) in the proneural zone (yellow background) regulate Delta expression (genetic schematic). Column 0 represents a row of R8 equivalence groups where the pre-R8 cell (dark blue) is selected from the group and emerges posterior of the MF to reside in column 1 (light blue background). The remaining columns are not indicated. Fully assembled R1–R8 PNs are depicted as Mid-expressing clusters (dark green) in the posterior (P) region (light green background). Although not shown, the R7 is located directly above the R8 PN in the center of clusters. We predict that the selected pre-SOP cells are situated close to the R7/R8 PN pair. The interleaved and scalloped configuration of a Dpp gradient filling the areas demarcated by solid and dashed black lines is shown to depict a pattern that may establish the coordinates where GPS-cells are selected before they transition to pre-SOP cells within the proneural zone. The illustrated genetic pathways below the eye disc are partly adopted from a review by Bao (2010).